

# Electromagnetic counterparts of supermassive black hole binaries resolved by pulsar timing arrays

Takamitsu Tanaka<sup>1\*</sup>, Kristen Menou<sup>1</sup>, and Zoltán Haiman<sup>1</sup>

<sup>1</sup>*Department of Astronomy, Columbia University, 550 West 120th Street, New York, NY 10027, USA*

25 November 2018

## ABSTRACT

Pulsar timing arrays (PTAs) are expected to detect gravitational waves (GWs) from individual low-redshift ( $z \lesssim 1.5$ ) compact supermassive ( $M \gtrsim 10^9 M_\odot$ ) black hole (SMBH) binaries with orbital periods of  $\sim 0.1 - 10$  yr. Identifying the electromagnetic (EM) counterparts of these sources would provide confirmation of putative direct detections of GWs, present a rare opportunity to study the environments of compact SMBH binaries, and could enable the use of these sources as standard sirens for cosmology. Here we consider the feasibility of such an EM identification. We show that because the host galaxies of resolved PTA sources are expected to be exceptionally massive and rare, it should be possible to find unique hosts of resolved sources out to  $z \approx 0.2$ . At higher redshifts, the PTA error boxes are larger, and may contain as many as  $\sim 100$  massive-galaxy interlopers. The number of candidates, however, remains tractable for follow-up searches in upcoming wide-field EM surveys. We develop a toy model to characterize the dynamics and the thermal emission from a geometrically thin gaseous disc accreting onto a PTA-source SMBH binary. Our model predicts that at optical and infrared frequencies, the source should appear similar to a typical luminous active galactic nucleus (AGN). However, owing to the evacuation of the accretion flow by the binary’s tidal torques, the source might have an unusually low soft X-ray luminosity and weak UV and broad optical emission lines, as compared to an AGN powered by a single SMBH with the same total mass. For sources at  $z \sim 1$ , the decrement in the rest-frame UV should be observable as an extremely red optical color. These properties would make the PTA sources stand out among optically luminous AGN, and could allow their unique identification.

**Key words:** black hole physics — gravitational waves — accretion, accretion discs — galaxies: active

## 1 INTRODUCTION

Over the last several years, the possibility of observing both the gravitational-wave (GW) and electromagnetic (EM) emission signatures of coalescing supermassive black hole (SMBH) binaries has received intense attention (Holz & Hughes 2005; Kocsis et al. 2006, 2007; Kocsis, Haiman & Menou 2008; Dotti et al. 2006; for an overview of proposed mechanisms for EM signatures, see Haiman et al. 2009; Schnittman 2011). The bursts of GWs emitted by such systems can now be predicted by numerical general relativity (Pretorius 2005; Baker et al. 2006; Campanelli et al. 2006), and are expected to be observed by current and future detectors. Of particular interest is the temporal evolution of the gravitational waveform, which can be used to extract the luminosity distance, help con-

strain the location of the source on the sky, and determine the masses and spins of the SMBHs. If an EM signature of the coalescence can also be identified, this would allow for a determination of the source redshift, turning merging black holes into “standard sirens” for probing cosmic expansion.<sup>1</sup> Such multi-messenger observations would also enable astronomical investigations of SMBHs whose masses, spins and orbital parameters are already known, presenting ideal laboratories for investigating accretion physics in active galactic nuclei (AGN). Furthermore, if major mergers of galaxies trigger luminous AGN activity (e.g., Sanders et al. 1988; Hernquist 1989; Carlberg 1990; Barnes & Hernquist 1991; Hernquist & Mihos 1995; Mihos & Hernquist 1996; Kauffmann & Haehnelt 2000; Hopkins et al. 2007, 2008),

<sup>1</sup> The importance of such GW+EM observations for cosmography was first discussed by Schutz (1986) in the context of merging neutron star binaries.

\* E-mail: takatanaka@astro.columbia.edu

then the characteristic EM emission promptly following the SMBH coalescence may herald the birth of a quasar (Tanaka, Haiman & Menou 2010).

To date, theoretical studies of EM signatures of GW-emitting SMBH binaries have largely centred on systems expected to be detected by the planned space-borne observatory *LISA*, i.e. systems with total mass  $\sim 10^{5-7}(1+z)^{-1}M_\odot$  out to  $z \gtrsim 10$ . A paramount feature of *LISA* for multi-messenger astronomy is the precision with which it is expected to determine the sky position of SMBH sources (Kocsis et al. 2006): to  $\lesssim 1^\circ$  (Vecchio 2004; Lang & Hughes 2008), or perhaps even to  $\lesssim 1'$  when spin-induced precession (Lang & Hughes 2006) or higher-order harmonics (McWilliams et al. 2010) are included in the analysis of the waveform.

In this paper, we evaluate the prospects of electromagnetically identifying GW-emitting SMBH binaries that are individually resolved by pulsar timing arrays (PTAs). PTAs will detect GWs from compact SMBH binaries that are more massive (total mass  $M \gtrsim 10^7 M_\odot$ ) and less compact (observer's-frame period of  $P_{\text{obs}} \sim 1$  yr) than those detectable by *LISA*. PTA detections will be comprised mostly of the collective background of the SMBH binary population at low redshift ( $z \lesssim 1.5$ ). However, theoretical population-synthesis studies (Sesana, Vecchio & Volonteri 2009; Sesana & Vecchio 2010; Kocsis & Sesana 2011) predict that the GW signals from the most massive and/or most nearby PTA sources will stick out above the background, and be individually resolved. According to those studies, resolved sources have chirp masses

$$\mathcal{M} \equiv M_1^{3/5} M_2^{3/5} M^{-1/5} = \eta^{3/5} M, \quad (1)$$

typically around  $\mathcal{M} \sim 10^{8.5} M_\odot$ . Above,  $M_2 \leq M_1$  are the masses of each member of the binary, and  $\eta \equiv M_1 M_2 / M^2 \leq 1/4$  is the symmetric mass ratio. The redshift probability distribution is poorly known, but is expected to decline steeply outside the range  $0.1 \lesssim z \lesssim 1.5$ , owing to the small volume at lower  $z$  and to the attenuation of the GW signal, as well as to the decline of the intrinsic SMBH merger rate at higher  $z$ . The orbits of PTA sources decay slowly, and most will not coalesce within a human lifetime – determining the masses and luminosity distances for the majority of sources will present a particularly difficult challenge. Another major challenge is the relatively poor sky-localization accuracy, which is expected to be  $\Delta\Omega \lesssim 3 \text{ deg}^2$  (if the contributions to the signal from individual pulsars are known; Corbin & Cornish 2010; hereafter CC10) to as large as  $\Delta\Omega \sim 40 \text{ deg}^2$  (if individual pulsar contributions cannot be extracted from the data; Sesana & Vecchio 2010; hereafter SV10).

In this paper, we investigate whether individually resolved PTA sources may be viable targets for EM identification. In particular, we address the following two questions:

(i) What is the average number  $N_g$  of candidate host galaxies — that is, interloping galaxies that could plausibly harbour the GW source — in a typical error box of a PTA detection? Of particular interest is whether there are plausible scenarios for detecting individually resolved sources with  $N_g < 1$ , i.e., cases where the source may be uniquely identified with an EM search of the three-dimensional PTA error box.

(ii) In cases where  $N_g > 1$ , what can be done to distinguish the true host galaxy of the source from the other interlopers? Motivated by the hypothesis that galaxy mergers can fuel AGN activity, we will consider the differences in thermal emission properties predicted by disc models of AGN powered by a compact SMBH binary as opposed to one powered by a solitary SMBH of the same total mass.

It is important to note that because most PTA sources will not merge within a human lifetime, many of the mechanisms hypothesized to elicit EM signatures for SMBH coalescences (e.g., gravitational recoil effect, loss of binary mass via GW emission, post-merger tidal response of a circumbinary accretion disc) are not applicable for PTA sources. Periodic emission modulated at the orbital frequency of the PTA source (e.g., Haiman et al. 2009 and references therein) and double-peaked broad emission lines (e.g., Gaskell 1996; Zhou et al. 2004; Bogdanović et al. 2008; Blecha & Loeb 2008; Boroson & Lauer 2009; Bogdanović, Eracleous & Sigurdsson 2009; Dotti et al. 2009; Tang & Grindlay 2009; Shen & Loeb 2010) have been previously considered in the literature as possible tell-tale EM features of compact SMBH binaries.

This paper is organized as follows. In §2, we provide a brief overview of the expected population of PTA-resolved SMBH binaries as well as the anticipated detection error box of such objects. We consider the error box prescriptions of SV10 and CC10, characterize the types of astronomical objects that are plausible hosts of a PTA-resolved binary, and estimate the number of such objects. In §3, we describe a toy model to calculate the dynamical state and thermal emission features of gas accreting onto a resolved SMBH binary. We discuss several features predicted by the model which, if observed, could help the EM identification of individually resolved PTA sources. We summarize our findings and offer our conclusions in §4.

Throughout this paper,  $c$  denotes the speed of light;  $G$  is the gravitational constant;  $h$  is Planck's constant;  $k_B$  is the Boltzmann constant;  $m_p$  is the mass of the proton; and  $\sigma_{\text{SB}}$  is the Stefan-Boltzmann constant.

## 2 PLAUSIBLE HOSTS OF PTA-RESOLVED BINARIES

As stated in §1, theoretical models predict that SMBH binaries individually resolved by PTAs are most likely to have masses of  $M \gtrsim 10^8 M_\odot$ , observed periods of  $P_{\text{obs}} \sim 1$  yr, and lie in a redshift range  $0.1 \lesssim z \lesssim 1.5$ . Given the PTA detection of such a GW-source binary, we wish to evaluate the number  $N_g$  of candidate galaxies that could plausibly host it. To this end, we will first review the volume of the error box in which we must look for the source, based on previous work on the source localization capability of PTAs. Then, we will evaluate the number of interloping host galaxies in the error box by estimating the number of (i) sufficiently massive dark matter halos, (ii) sufficiently luminous galaxies, and (iii) AGN. We adopt a standard  $\Lambda$ CDM cosmology with  $h = 0.70$ ,  $\Omega_m = 0.27$ ,  $\Omega_\Lambda = 1 - \Omega_m$ ,  $\Omega_b = 0.046$ , and  $\sigma_8 = 0.81$  (WMAP 7-year results, Jarosik et al. 2011).

## 2.1 The PTA Error Box

We consider two different estimates of the size of the error box of PTA-resolved sources. The first is based on the calculations by SV10, who assumed that the contributions to the signal from GW perturbations at the individual pulsars (the so-called “pulsar term”) cannot be extracted from the PTA data. The location on the sky of a resolved source can then be determined within an error of  $\Delta\Omega \sim 40 \text{ deg}^2 (\text{SNR}/10)^{-2}$ , where SNR is the signal-to-noise ratio. The error of the signal amplitude  $A \propto \mathcal{M}^{5/3} D_L^{-1}$  will be of order  $\sim 30\%$ . Given the wide spread in chirp mass distribution predicted by population synthesis models of resolved sources, in the absence of an independent measurement of  $\mathcal{M}$  the only constraint on  $D_L$  comes from the maximum distance at which PTAs are expected to detect individually resolved sources. The population synthesis models (Sesana, Vecchio & Volonteri 2009; Kocsis & Sesana 2011) predict that the majority of resolved sources will lie below a maximum redshift  $z_{\text{max}} \sim 1.5$ , or a luminosity distance below  $D_{L,\text{max}} \lesssim 10^4$  Mpc. This “worst-case” error box has a comoving volume of

$$\Delta V^{(\text{SV})} \sim 3 \times 10^8 \left( \frac{\Delta\Omega}{40 \text{ deg}^2} \right) \text{Mpc}^3. \quad (2)$$

More optimistic numbers are obtained by CC10, who suggested that utilizing information on the distances to individual pulsars in the array can greatly enhance the measurement capabilities of PTAs. They concluded that if the individual pulsar term can be extracted from the signal, then this would double the signal power and enable direct measurement of the chirp mass. They estimate that for a system with SNR = 20 (corresponding to a detection of SNR = 10 without pulsar distance information), a resolved source can be localized with distance and angular errors of  $\Delta D_L/D_L < 20\%$  and  $\Delta\Omega < 3 \text{ deg}^2$ , respectively. Noting that the comoving distance  $D(z)$  in the relevant redshift range can be analytically approximated<sup>2</sup> as  $D \approx cH_0^{-1}z(1-0.2z)$ , we may estimate the error box in the CC10 scenario as

$$\Delta V^{(\text{CC})} \approx 1.2 \times 10^6 z^3 (1-0.2z)^3 \left( \frac{\Delta\Omega}{3 \text{ deg}^2} \right) \left( \frac{\Delta D_L/D_L}{20\%} \right) \text{Mpc}^3. \quad (3)$$

## 2.2 Interloper Counts

Where does an individually resolved PTA source live? The mass  $M$  of a nuclear SMBH is known to correlate with the velocity dispersion  $\sigma$  of the host galaxy (the “ $M - \sigma$  relation”; Ferrarese & Merritt 2000; Gebhardt et al. 2000; Tremaine et al. 2002), as well as with the stellar luminosity of the host (the “ $M - L$  relation”; Kormendy & Richstone 1995; Magorrian et al. 1998; Häring & Rix 2004; Lauer et al. 2007); with more massive halos and luminous galaxies hosting more massive SMBHs. That resolved PTA sources are expected to be exceptionally massive ( $M \gtrsim 10^8 M_\odot$ ) implies that the host should be a

giant elliptical galaxy or be among the most massive spiral galaxies (with velocity dispersion  $\sigma \gtrsim 200 \text{ km s}^{-1}$  of the spheroid component; e.g. Gültekin et al. 2009).

Assuming that SMBH binaries are able to overcome the “final parsec” problem (e.g., Escala et al. 2005; Mayer et al. 2007; Callegari et al. 2009; Colpi et al. 2009; Hayasaki 2009; see, however, Lodato et al. 2009), we expect the PTA host galaxy to be the product of a relatively recent merger. A natural question to ask is whether such galaxies typically lie in the field, or in the centre of a cluster. We can answer this question qualitatively by considering the dependence of the major merger rates of the most massive dark matter halos on their environments. Analyses by Fakhouri & Ma (2009) and Bonoli et al. (2010) of the Millennium simulation results (Springel et al. 2005) indicate that while the rate of major mergers is enhanced in over-dense environments, this effect is weak: for halo masses and redshifts of interest ( $M \gtrsim 10^{13} M_\odot$  and at  $z \lesssim 1.5$ ), the ratio of merger rates between the most and least over-dense regions is of order unity. We interpret this result to mean that there is no strong reason to search for PTA sources in galaxy clusters as opposed to those in the field.

### 2.2.1 The most massive halos

One conservative way to estimate the number  $N_g$  of host galaxy candidates in the error box is to simply count the dark matter halos that are massive enough to plausibly harbour the source SMBH binary. We use the observational results of Dutton et al. (2010), who infer a double-power-law fit for the relation between the SMBH mass  $M$  and the host halo mass  $M_{\text{halo}}$  for local elliptical galaxies. We extrapolate their results to higher redshifts by postulating the canonical  $z$ -dependence based on the theory for spherically collapsing halos (see, e.g., Wyithe & Loeb 2003),

$$M_{\text{halo}}(M, z) \propto F(z) \equiv \sqrt{\frac{d(z)}{d(0)} \frac{\Delta_c(0)}{\Delta_c(z)}}, \quad (4)$$

where  $d(z) = -[(\Omega_m/\Omega_\Lambda)(1+z)^3 + 1]^{-1}$  and  $\Delta_c(z) = 18\pi^2 + 82d(z) - 39d^2(z)$ . We obtain

$$M_{\text{halo}} \approx 2.3 \times 10^{13} M_9^{0.75} \left[ \frac{1}{2} + 13M_9^{1.77} \right]^{0.50} F(z) M_\odot, \quad (5)$$

where  $M_9 \equiv M/(10^9 M_\odot)$ . We estimate the number of candidate host halos inside the three-dimensional PTA error box by integrating the halo mass function of Jenkins et al. (2001; their equation 9) above  $M_{\text{halo}}$ .

The most massive halos with  $M_{\text{halo}} \gtrsim \text{few} \times 10^{14} M_\odot$ , which are associated with galaxy clusters, may be expected to contain more than one plausible host galaxy. Since the halo mass function at  $M_{\text{halo}} \gtrsim \text{few} \times 10^{14} M_\odot$  drops much more steeply than linear with mass, whereas the sub-halo mass function increases less steeply than linear (Giocoli et al. 2010), most galaxies with halo masses  $\sim 10^{13} M_\odot$  will reside in the field, rather than in groups and clusters. The multiple occupancy of massive galaxies in the most massive halos will then represent only a small increase in our total counts of interlopers. As the purpose of the exercise in this section is to give order-of-magnitude estimates for interlopers, we will neglect sub-halos in our analysis.

<sup>2</sup> This fitting formula has an error of less than 1% in  $D$  at  $z \leq 1.4$  and roughly 5% at  $z = 1.9$ . It is provided for the reader's convenience; all distance and volume calculations in this paper are performed using exact expressions.

### 2.2.2 The brightest galaxies

A second way to estimate the number of candidate host galaxies is through the  $M - L$  relation, where  $L$  is the luminosity of the host galaxy. Of particular interest is the fact that the  $M - L$  relation and the  $M - \sigma$  relations are discrepant at the high-mass end (here  $\sigma$  denotes the velocity dispersion of the host). The former predicts higher masses for the most massive SMBHs, and higher number densities for fixed BH mass (Lauer et al. 2007, and references within). This therefore results in a greater number of individually resolvable PTA sources (Sesana, Vecchio & Volonteri 2009).

Since  $\sigma$  is used to infer  $M_{\text{halo}}$ , we expect that for a fixed SMBH mass, the number of expected interloping host galaxies, inferred from the  $M - L$  relation, would also be greater than the number of halos, inferred from the  $M - \sigma$  and  $\sigma - M_{\text{halo}}$  relations.

To evaluate this different estimate quantitatively, we adopt the  $M - L$  relation found by (Lauer et al. 2007) for the most luminous core galaxies in their sample,

$$M_V \approx -22.0 - 1.8 \log_{10} M_9, \quad (6)$$

where  $M_V$  is the  $V$ -band magnitude of the host galaxy.

To compute the number of sufficiently luminous galaxies, we use the results of Gabasch et al. (2004, 2006), who measured the luminosity function in multiple wavelength bands between 150 – 900 nm, and studied the redshift evolution in each band out to  $z \gtrsim 2$ . The luminosity function is given in the form of a standard Schechter function (Schechter 1976),

$$\begin{aligned} \phi(M_V) = & \frac{2}{5} (\ln 10) \phi^* \left[ 10^{(2/5)(M_V^* - M_V)} \right]^{\alpha_0 + 1} \\ & \times \exp \left[ -10^{(2/5)(M_V^* - M_V)} \right]. \end{aligned} \quad (7)$$

They set a constant value for the parameter  $\alpha_0$  while fitting  $M_V^*$  and  $\phi^*$  to a power-law redshift dependence of the form

$$M_V^*(z) = M_{V,0}^* + A \ln(1+z), \quad (8)$$

$$\phi^*(z) = \phi_0^* (1+z)^B. \quad (9)$$

The five fitting parameters ( $\alpha_0, M_{V,0}^*, \phi_0^*, A, B$ ) vary with the wavelength band of the luminosity function. Because the Gabasch et al. results do not have fits for the  $V$ -band, we interpolate the parameters between neighbouring bands to obtain the following values:  $\alpha_0 \approx -1.3$ ,  $M_{V,0}^* \approx -21.1$ ,  $\phi_0^* \approx 6.2 \times 10^{-3} \text{ Mpc}^{-3} M_V^{-1}$ ,  $A \approx -1.18$ , and  $B \approx -1.05$ .

### 2.2.3 The brightest AGN

Finally, a third method to identify plausible hosts is to search for AGN that are luminous enough to be plausibly powered by a  $M \sim 10^9 M_\odot$  SMBH. AGN activity is an ideal scenario for identifying the EM counterparts of PTA sources, as the interaction between a compact SMBH binary and its accretion flow provide a natural physical mechanism for eliciting a smoking-gun EM signature. However, a significant uncertainty with this approach is whether the host of a resolved PTA source is likely to be undergoing an observable AGN episode. While multiple studies have suggested that galaxy mergers trigger AGN activity (refs. in §1) whether the two phenomena are causally related remains an open question.

Recently, Schawinski et al. (2011) suggested that the low Sersic indices in most X-ray-selected AGN hosts at  $1.5 < z < 3$  indicate that they are disc galaxies, and therefore unrelated to mergers (see, however, Governato et al. 2009, who suggest mergers can result in disc galaxies). Further, even if one accepts that there exists a direct causal connection between galaxy mergers and luminous AGN activity, it is uncertain whether such a trend extends to the most massive galaxies at  $z < 1.5$ . The mass fraction of cold gas in massive galaxies tend to decrease toward lower redshift, and gas-poor “dry” mergers are thought to play an important (if not dominant) role in the assembly of giant elliptical galaxies at  $z < 1$ , in the field as well as in clusters (van Dokkum 2005; Lin et al. 2008, 2010). On the other hand, the amount of gas required to fuel a luminous AGN episode is a small fraction of the total gas content of even very gas-poor galaxies; the most luminous known AGN are situated in giant elliptical galaxies; a plurality of mergers of massive galaxies at  $z < 1$  are gas-rich (Lin et al. 2008); many early-type galaxies identified as undergoing a dry merger have been found to contain detectable amounts of gas in followup HI observations (e.g., Donovan, Hibbard & van Gorkom 2007; Sánchez-Blázquez et al. 2009); and even though the hosts of the most luminous quasars tend to be ellipticals, they are not exclusively so in the SMBH mass regime of interest ( $M \gtrsim 10^8 M_\odot$ ; e.g., Percival et al. 2001; Floyd et al. 2004; Zakamska et al. 2006, and references therein). We conclude that PTA sources powering luminous AGN activity is a plausible scenario, and not merely an expedient assumption.

We parameterize the minimum luminosity for the AGN counterpart in terms of the Eddington luminosity  $L_{\text{Edd}}(M) = 4\pi G M \mu_e m_p c / \sigma_T$ , where  $\mu_e$  is the mean molecular weight per electron and  $\sigma_T$  is the Thomson cross section:

$$L_{\text{min}}(M) = f_{\text{min}} L_{\text{Edd}}(M). \quad (10)$$

We choose  $f_{\text{min}} = 10^{-2}$  for our minimum Eddington ratio  $L/L_{\text{Edd}}$ , motivated by the fact that this quantity is observed to peak at  $L/L_{\text{Edd}} \sim 0.1 - 0.3$  (e.g., Kollmeier et al. 2006).

In order to estimate the number of AGN that are bright enough to correspond to a PTA source with mass  $M$ , we adopt the observationally motivated fits to the AGN luminosity function given by Hopkins, Richards & Hernquist (2007; their equations 6, 18 and 20, and Table 3).

Note that although the Eddington ratio distribution and the luminosity function cited above are expressed in terms of the bolometric luminosity, they are actually proxies for the optical luminosity. Hopkins, Richards & Hernquist (2007) noted that their bolometric luminosity function is effectively equivalent to the optical luminosity function, and Kollmeier et al. (2006) uses the flux at 510 nm to estimate the bolometric luminosity. Our AGN interlopers are therefore optically luminous AGN, and we assume nothing a priori about the X-ray and UV emission of accreting PTA sources. We will discuss the importance of searching for the EM counterpart at optical wavelengths in §3.3.

## 2.3 Expected Counts of Interloping Galaxies

If the individual pulsar contributions to the signal cannot be extracted, as in the SV10 scenario, then the chirp mass

and luminosity distance of the resolved source cannot be independently known, and the source can only be localized within a solid angle  $\Delta\Omega$ . The only constraints on  $\mathcal{M}$  and  $D_L$  are then model-dependent, and come from theoretical expectations for the population of resolvable sources, given the detection threshold of the array. The upper end of the chirp mass distribution of SMBH binaries, along with the detector sensitivity, sets a maximum luminosity distance  $D_{L,\max}$  (equivalently,  $z_{\max}$ ). Similarly, the chirp mass distribution in the local Universe determines a minimum chirp mass  $\mathcal{M}_{\min}$  required for a PTA source to be resolved. Note that since  $M = \eta^{-3/5} \mathcal{M} \geq 2^{6/5} \mathcal{M}$ , the quantity  $\mathcal{M}_{\min}$  also sets a lower limit  $M_{\min} \approx 2.3 \mathcal{M}_{\min}$  on the gravitational mass.

The number of interloping halos can be expressed as

$$N_{\text{halo}}^{(\text{SV})} = \frac{\Delta\Omega}{4\pi} \int_0^{z_{\max}} \int_{M_{\text{halo}}(M_{\min}, z)}^{\infty} \frac{dn_{\text{halo}}}{dM_{\text{halo}}} dM_{\text{halo}} \frac{dV}{dz} dz, \quad (11)$$

where  $n$  is the comoving number density of dark matter halos, and  $dV/dz = 4\pi D_L^2 dD_L/dz$  is the comoving volume element. The lower limit of the integral over halo mass is given by equation 5. Similarly, the numbers of interloping galaxies and AGN are given by the expressions

$$N_{\text{gal}}^{(\text{SV})} = \frac{\Delta\Omega}{4\pi} \int_0^{z_{\max}} \int_{-\infty}^{M_V(M_{\min}, z)} \phi dM_V \frac{dV}{dz} dz, \quad (12)$$

$$N_{\text{AGN}}^{(\text{SV})} = \frac{\Delta\Omega}{4\pi} \int_0^{z_{\max}} \int_{L_{\min}(M_{\min})}^{\infty} \frac{dn_{\text{AGN}}}{dL} dL \frac{dV}{dz} dz. \quad (13)$$

The limits of integration over luminosity are taken from equations 6 and 10.

We show in Figure 1 the estimated number of interlopers for the worst-case error box in the SV10 scenario, assuming  $\Delta\Omega = 40 \text{ deg}^2$ , as a function of the maximum redshift  $z_{\max}$  and minimum BH binary mass  $M_{\min}$ . Panels (a), (b) and (c) show the isonumber contours of the expected number of interloping massive halos, luminous galaxies and luminous AGN, respectively. All three methods to estimate the number of interlopers yield on the order of  $N_g \gtrsim 10^2$  for PTA sources with  $M > 10^9 M_{\odot}$ , if the redshift range is restricted to  $z_{\max} \sim 1$ .

The difference in the number of interlopers between the top two panels (halos vs. galaxies) for the most massive SMBHs arises because the observed SMBH samples yield an internally inconsistent set of  $M - \sigma$ ,  $L - \sigma$  and  $M - L$  relations, as mentioned above. While the interpretation of this inconsistency is beyond the scope of our paper, we note that Tundo et al. (2007) discussed this issue, and concluded that the intrinsic scatter in the relations produces a selection bias: using the observed BH samples yields a biased  $L - \sigma$  relation (too low  $L$  for given  $\sigma$ ). This suggests that the  $M - L$  galaxy relation we adopted may also be biased and it under-predicts  $L$ ; correcting this bias would decrease the number of galaxy interlopers.

If the GW signal can be used to constrain  $\mathcal{M}$  and  $D_L$  of the source via statistical inference, as suggested by CC10, then the numbers of interloping halos, luminous galaxies and

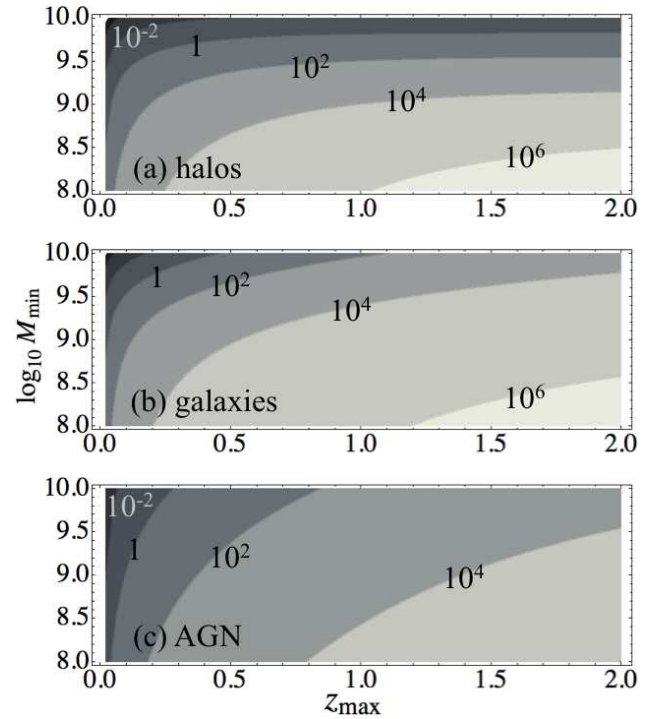


**Figure 1.** Estimates of the number of interloping host objects — (a) massive dark matter halos, (b) luminous galaxies, and (c) luminous AGN — in the conical error volumes suggested by SV10. The extent of the error volume is limited by  $z_{\max}$ , the maximum redshift at which PTAs can resolve an individual source, and the angular localization  $\Delta\Omega = 40 \text{ deg}^2$ . The number of interlopers is calculated by assuming a minimum SMBH mass  $M_{\min}$ , which then sets the minimum host mass/luminosity through equations 5, 6, and 10.

AGN are given by

$$N_{\text{halo}}^{(\text{CC})}(z) = \frac{\Delta\Omega}{4\pi} \int_{z_-}^{z_+} \int_{M_{\text{halo}}(M_{\min}, z)}^{\infty} \frac{dn_{\text{halo}}}{dM_{\text{halo}}} dM_{\text{halo}}, \quad (14)$$

$$N_{\text{gal}}^{(\text{CC})}(z) = \frac{\Delta\Omega}{4\pi} \int_{z_-}^{z_+} \int_{-\infty}^{M_V(M_{\min}, z)} \phi dM_V \frac{dV}{dz} dz, \quad (15)$$

$$N_{\text{AGN}}^{(\text{CC})}(z) = \frac{\Delta\Omega}{4\pi} \int_{z_-}^{z_+} \int_{L_{\min}(M_{\min})}^{\infty} \frac{dn_{\text{AGN}}}{dL} dL, \quad (16)$$

respectively. Above, the redshifts  $z_{\pm} = z(D_L \pm \Delta D_L)$  bound the radial extent of the error box. We adopt  $\Delta\Omega = 3 \text{ deg}^2$  and  $\Delta D_L/D_L = 20\%$ . We ignore errors due to weak lensing, which are expected to be on the order of several percent for sources with  $z \lesssim 1.5$  (Kocsis et al. 2006; Hirata, Holz & Cutler 2010; Shang & Haiman 2011). We do not place an upper limit on the host halo mass (or on the host galaxy luminosity). In principle, such an upper limit could be computed, given PTA's observational error on the chirp mass and the spread in the ratio between the chirp mass and the gravitational mass of the binary (i.e., from the model-dependent mass ratio distribution of resolved sources). For example, CC10 provide a chirp mass error estimate of  $\Delta\mathcal{M} \sim 5\%$ . Converting the chirp mass to the gravitational mass, however, can introduce a large uncertainty, e.g. a factor of  $\sim 2$  depending on whether the mass ratio is 0.1 or 1. Since the number density of interlopers decrease

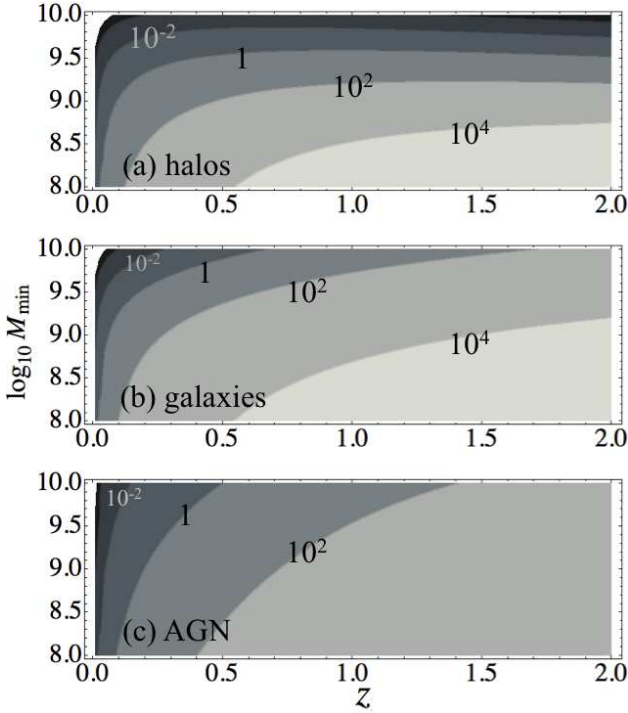


**Figure 2.** Same as Figure 1, except that the error volume is calculated from the results of CC10, who assumed that the pulsar term of the GW signal can be used to infer the luminosity distance to the source binary. The error box is limited by the uncertainty  $\Delta D_L/D_L = 20\%$  in the luminosity distance to the source, and the angular localization  $\Delta\Omega = 3 \text{ deg}^2$ . Note that whereas the horizontal axis in Figure 1 showed the maximal PTA detection range  $z_{\text{max}}$ , here it denotes the actual redshift  $z$  of the source.

rapidly with increasing halo mass (or luminosity), this simplification should not affect our estimates.

In Figure 2, we plot the number of interloping host candidates against the source redshift  $z$ . Not surprisingly, the prospects for EM identification improve dramatically in the CC10 scenario. For massive ( $M \gtrsim 10^9 M_\odot$ ) resolved PTA sources, we anticipate that the error box will contain a single host candidate at  $z \lesssim 0.2$ , and several hundred at  $z \lesssim 0.7$ . We expect only a single group-sized halo ( $M \gtrsim \text{few} \times 10^{13} M_\odot$ ) in the error box at any redshift in the CC10 scenario. Note that the number  $N_g$  of interlopers is not necessarily a monotonically increasing function of  $z$ , as the decline in the number densities of the interloping objects (in particular massive halos) competes with the increase in the comoving size of the error boxes.

Our simple calculations show that in the scenario of CC10, resolved PTA sources with  $M \gtrsim 10^9 M_\odot$  and  $z \lesssim 0.5$  are likely to have at worst dozens of interlopers in the error box. With this low number, one could conceivably perform follow-up observations of each individual candidate. If, on the other hand, luminosity distances to the source cannot be determined, this number increases to  $\sim 10^3$ , suggesting that it will become extremely difficult to electromagnetically identify the source in the absence of an obvious, tell-tale EM signature.

In practice, the number of interloping galaxies may be somewhat larger than the value computed by equations 11–16. The halo mass of any given candidate host system

will not be known a priori, and the intrinsic scatter in the  $M_{\text{SMBH}} - M_{\text{halo}}$  ( $M_{\text{SMBH}} - \sigma_{\text{host}}$ ) relation will lower the minimum halo mass threshold for candidacy. On the other hand, the simple calculations presented here do not consider detailed demographic properties of resolved PTA sources and plausible hosts, such as the presence of a nuclear stellar core (Makino 1997; Ravindranath, Ho & Filippenko 2002; Milosavljević et al. 2002; Volonteri, Madau & Haardt 2003) or galaxy morphology. Including such factors in the analysis will narrow the field of candidate hosts.

As we argue in 3.3, candidate AGN counterparts may be further vetted by examining their UV and X-ray emission for features indicative of a central SMBH binary (see also Sesana et al. 2011 for an in-depth discussion of possible high-energy signatures for pre-decoupling — i.e.,  $t_{\text{GW}} > t_\nu$  — PTA sources). In addition, PTA sources are sufficiently nearby that it should be possible to observe an interloping AGN together with its host galaxy. It should therefore be possible to combine the AGN emission, the galaxy luminosity and the inferred SMBH mass to cross-check candidate counterparts.

### 3 ACCRETION DISCS AROUND PTA-SOURCE BINARIES

Motivated by the results of the previous section that the number of plausible host galaxies in the PTA error box may be tractable for follow-up EM searches, we next model the EM emission properties of SMBH binaries detectable by PTAs. We focus our attention on SMBH binaries that are undergoing luminous accretion, as these are the most promising class of objects for EM identification.

Normalizing the binary mass  $M$  and rest-frame period  $P$  to the typical orders of magnitude expected of resolved PTA sources,  $M = 10^9 M_\odot M_9$  and  $P = 1 \text{ yr } P_1$ , we write the semi-major axis for the source binary as

$$\begin{aligned} a(M, P) &= 101 M_9^{-2/3} P_1^{2/3} \frac{GM}{c^2} \\ &= 2.23 \times 10^{-2} M_9^{1/3} P_1^{2/3} \text{ pc}. \end{aligned} \quad (17)$$

Binaries detectable by PTAs have long overcome the so-called “final parsec” problem. The rest-frame time to merger for a binary with mass  $M$  and semi-major axis  $a$ , driven by GW emission alone, is

$$\begin{aligned} t_{\text{merge}} &\leq \frac{5}{256} \frac{c^5}{G^3 M^3} \frac{a^4}{\eta} \\ &= 1.9 \times 10^3 M_9 \eta_{1:4}^{-1} \left( \frac{a}{10^2 GM/c^2} \right)^4 \text{ yr} \\ &= 2.0 \times 10^3 M_9^{-5/3} \eta_{1:4}^{-1} P_1^{8/3} \text{ yr} \end{aligned} \quad (18)$$

(Peters 1964). Because typical resolved sources have  $M/\mathcal{M} = \eta^{-3/5} \sim 3$ , we normalize the symmetric mass ratio  $\eta \equiv (M_2/M_1)/[1 + M_2/M_1]^2$  to the value  $\eta_{1:4} \equiv \eta(M_2/M_1 = 0.25) = 0.16$ . Note that our ad hoc translation between  $M$  and  $\mathcal{M}$  is not very sensitive to the value of  $q$ ; the ratio  $M/\mathcal{M}$  varies by less than a factor of two in the range  $0.1 \leq M_2/M_1 \leq 1$ . The upper bound in equation 18 corresponds to binaries in circular orbits, with eccentric orbits merging faster. Recent work has shown that binaries may have eccentricities as high as  $\sim 0.6$  at decoupling

(Roedig et al. 2011; see also Armitage & Natarajan 2005; Cuadra et al. 2009). Thus, typical PTA-resolved sources will coalesce on scales of  $\sim 10^3$  years. However, exceptionally compact sources will coalesce on scales of several years; for example, a binary with  $P = 0.1$  yr — approximately the lowest binary period that is expected to be observable with PTAs — will merge in  $t_{\text{merge}} \sim 4$  yr.

The tidal torques of the compact SMBH binary provide a particularly promising mechanism for producing a tell-tale observable feature. Theoretical calculations (Goldreich & Tremaine 1980; Artymowicz et al. 1991; Artymowicz & Lubow 1994; Armitage & Natarajan 2002; Bate et al. 2003; Hayasaki, Mineshige & Sudou 2007; MacFadyen & Milosavljević 2008; Cuadra et al. 2009; Chang et al. 2010) robustly predict that in geometrically thin circumbinary accretion discs, binary torques can open an annular, low-density gap around the orbit of the secondary. The gas inside the gap accretes onto the individual SMBHs while the gas outside is pushed outward by the tidal torques. The binary’s tidal torques transfer orbital angular momentum into the outer disc, causing the binary’s orbit to shrink gradually while maintaining a roughly axisymmetric circumbinary gap.

Following Milosavljević & Phinney (2005), we parametrize the location of the outer edge of the gap,  $R \approx 3^{2/3}a \approx 2.08a$  (Artymowicz et al. 1991), as  $R_\lambda \equiv 2\lambda a$ , where  $\lambda \sim 1$  is a dimensionless parameter. We are interested in circumbinary discs that are truncated inside  $R_\lambda \sim 200M_9^{-2/3}P_1^{2/3}GM/c^2$ . Below, we model surface density profiles and thermal emission spectra of such discs, and consider thermal emission due to leakage of gas into the cavity and onto individual SMBHs.

### 3.1 Disk Properties and Binary Decay

#### 3.1.1 Disk around a solitary SMBH

Adopting a geometrically thin, thermal gray-body disc model (e.g., Blaes 2004; Milosavljević & Phinney 2005), we estimate the properties of circumbinary discs around resolved PTA sources. As a reference model, let us consider a disc around a solitary SMBH.

Disks whose kinematic viscosities  $\nu$  scale with the total pressure  $p = p_{\text{gas}} + p_{\text{rad}}$  are known to be thermally unstable (Shakura & Sunyaev 1976; Pringle 1976; see, however, Hirose, Krolik & Blaes 2009). We therefore adopt a prescription in which the kinematic viscosity scales with gas pressure (a.k.a. the “ $\beta$ -disc” model), which is known to be thermally stable:

$$\nu = \frac{2}{3} \frac{\alpha P_{\text{gas}}}{\rho \Omega} = \frac{2}{3} \frac{\alpha k_B T}{\mu m_p \Omega}. \quad (19)$$

This viscosity prescription is also consistent with previous analyses of thin circumbinary discs (Milosavljević & Phinney 2005; Tanaka & Menou 2010). However, an important caveat is that radiation pressure-dominated discs may be *viscously* unstable (Lightman & Eardley 1974; Piran 1978; Hirose, Blaes & Krolik 2009); our results are conditional on this theoretical uncertainty. We choose  $\alpha = 0.3$  as the fiducial value, and write  $\alpha_{0.3} = \alpha/0.3$ . We assume that

shear viscosity is the dominant mechanism for the transport of angular momentum.

The surface density  $\Sigma$  and the mid-plane temperature  $T$  of the disc are obtained through the following equations:

$$\Xi(\Omega, T_p) \sigma_{\text{SB}} T_p^4 = \frac{9}{8} \nu \Sigma \Omega^2 \quad (20)$$

$$T_p^4 = \frac{4}{3\tau} T^4 \quad (21)$$

$$\tau = \theta \kappa \Sigma \quad (22)$$

$$\Sigma = \frac{\dot{M}}{3\pi\nu}. \quad (23)$$

Above,  $\Xi$  is the deviation of the bolometric flux from black-body due to the photons being thermalized above the mid-plane (see, e.g., Blaes 2004),  $T_p$  is the temperature of the thermalization photosphere, and  $\tau$  is the optical depth between the mid-plane and the thermalization photosphere. The dimensionless parameter  $\dot{m} \equiv \dot{M}/\dot{M}_{\text{Edd}}$  describes the accretion rate in units of the Eddington rate, assuming a radiative efficiency of 0.1, i.e.  $L_{\text{Edd}} = 0.1\dot{M}_{\text{Edd}}c^2$ . The quantity  $\theta$  is a porosity factor that relates the surface density to the optical depth. We set it to 0.2 following Turner (2004) and express our results in terms of  $\theta_{0.2} = \theta/0.2$ ; however, most disc properties are not very sensitive to this parameter.

The disc scale height  $H$  is evaluated in the usual way:

$$c_s^2 \equiv \frac{P}{\rho} = H^2 \Omega^2 + 4\pi G \Sigma H, \quad (24)$$

where  $c_s \equiv \sqrt{P/\rho}$  is the isothermal sound speed calculated from the total pressure  $P = P_{\text{gas}} + P_{\text{rad}}$ , and the volume density  $\rho$  of the disc is given by  $\rho = \Sigma/H$ . The second term on the right-hand side of equation 24 is due to the disc’s self-gravity (e.g., Paczynski 1978).

In the regions of interest, the dominant source of opacity is electron scattering, and vertical pressure in the disc is due primarily to radiation pressure. In this regime, the gray-body factor  $\Xi$  can be approximated as  $\Xi \approx 0.17(\Omega \text{ yr})^{1/2} [T_p/(10^4 \text{ K})]^{-15/8}$  (Tanaka & Menou 2010), and with a little algebra we obtain the surface density profile in the disc:

$$\Sigma(R) \approx 1.3 \times 10^6 \text{ g cm}^{-2} \left( \frac{R}{100GM/c^2} \right)^{-6/17} \times M_9^{16/85} \dot{m}^{36/85} \alpha_{0.3}^{-4/5} \theta_{0.2}^{-1/5} \dots \quad (25)$$

A steady-state disc far from the central object satisfies  $\dot{M} = 3\pi\nu\Sigma = \text{constant}$ , and so we have  $\nu \propto \Sigma^{-1} \propto R^{6/17}$ .

#### 3.1.2 Circumbinary discs around orbit-decaying binaries

After a circumbinary gap is opened, the SMBH binary undergoes several stages of orbital decay. Let us briefly examine the different stages, and the orbital evolution timescale (or residence time)  $t_{\text{res}} \equiv a/|da/dt|$  for each. Our goal here is to describe the structure of a dense gaseous annulus, extending at least a factor of few in radius, that is created around the PTA source. The annulus results from inward migration of the binary from larger radii in a more extended accretion disc. For a more thorough discussion of the orbital decay of SMBHB binaries, through various physical regimes in a thin disc, see, e.g. Haiman, Kocsis & Menou (2009).

We begin with disc-driven orbital decay, in which the



binary's tidal torques transfer its orbital angular momentum to the surrounding gas. At large orbital separations, the mass of the gas at the edge of the cavity far exceeds the mass of the secondary. In this regime, analogous to disc-dominated Type II migration for proto-planets, the binary's orbital evolution is limited only by the rate at which the nearby gas can transport away angular momentum, i.e.

$$t_{\text{res}}^{(\text{disc})} = t_{\nu}(R_{\lambda}) = \frac{2R_{\lambda}^2}{3\nu(R_{\lambda})}. \quad (26)$$

The tidal torques prevent the gas from flowing inward of  $R_{\lambda}$ , and so the region inside the gap is starved. Any gas that is initially present will be depleted on the local viscous timescale (Chang et al. 2010). In standard steady-state thin-disc models the viscosity is an increasing function of radius, so this drainage occurs on timescales shorter than that of the binary's orbital decay.

When the mass of the secondary becomes comparable to the local disc mass, the orbital decay slows down with respect to the local viscous time. The gas piles up immediately outside the cavity, forming a decretion region in which the viscous torque  $\mathcal{T}_{\nu} = 3\pi\nu\Sigma\Omega R^2$  is nearly constant with radius (Pringle 1991). We apply the analytic model of Ivanov, Papaloizou & Polnarev (1999) to calculate the residency time for this secondary-dominated migration stage:

$$t_{\text{res}}^{(\text{sec})} = \frac{\eta M}{4\pi R_{\lambda}^2 \Sigma(R_{\lambda})} t_{\nu}(R_{\lambda}). \quad (27)$$

Note that there are two competing effects influencing  $t_{\text{res}}^{(\text{sec})}$ : the decay slows down as the local disc mass decreases with respect to the secondary, but this is mitigated to a small extent by the fact that  $\Sigma$  outside the cavity increases due to pile-up. The enhancement of  $\Sigma$  relative to that of a disc around a solitary SMBH of the same mass as the binary (equation 25) has the functional form (Ivanov, Papaloizou & Polnarev 1999)

$$\frac{\Sigma^{(\text{binary})}}{\Sigma^{(\text{solitary})}} = \left\{ 1 + A \left[ 1 - \left( \frac{R_{\lambda}}{R_{\lambda}^{(\text{disc/sec})}} \right)^{1/2} \right]^B \right\} \left( \frac{R}{R_{\lambda}} \right)^{-1/2} \quad (28)$$

in the neighbourhood  $R \gtrsim R_{\lambda}$ . Above,  $R_{\lambda}^{(\text{disc/sec})}$  is the radius of the cavity when the transition from disc-dominated to secondary-dominated migration occurs, i.e. when  $\eta M = 4\pi R_{\lambda}^2 \Sigma(R_{\lambda})$ . For reasonable parameter values,  $R_{\lambda}^{(\text{disc/sec})} > 10^3 GM/c^2$ . The dimensionless quantities  $A$  and  $B$  in equation 28 depend on the viscosity and mass profiles of the disc (see Ivanov, Papaloizou & Polnarev 1999, for details). We typically find that  $A \sim 4$  and  $B \sim 0.2$  in our disc models; i.e., the fractional surface density enhancement during secondary-dominated migration is no greater than  $(1+A)^B \sim 1.4$ .

At yet smaller separations, the binary's orbital evolution begins to be driven by GW emission. Since binaries of interest here are far from merging, GW emission can be approximated by the leading term in the Newtonian quadrupole. For circular orbits, the residence time is given by Peters (1964)

$$t_{\text{res}}^{(\text{GW})} = 4t_{\text{merge}} = \frac{5}{64} \frac{c^5}{G^3 M^3} \frac{a^4}{\eta}. \quad (29)$$

As the binary's orbital decay accelerates due to GW emission, the pileup caused by secondary-dominated migration

spreads out. Past the point where  $t_{\text{res}}^{(\text{GW})} \approx t_{\nu}(R_{\lambda})$ , the binary begins to outrun the disc, as the decay timescale for  $a$  becomes rapidly shorter than that on which the disc can viscously spread.

Let us now discuss the gravitational stability of the disc, based on the stability criteria of a radiation-pressure dominated fluid summarized by Thompson (2008). If the radiative diffusion timescale is much shorter than the dynamical timescale, then the radiation pressure does not stabilize the fluid and gravitational fragmentation occurs on the same length scales as it would in the absence of radiation pressure. If the radiative diffusion timescale is much longer than the dynamical time, which we find to be the case for our disc models, then radiation pressure acts to make the fluid more Jeans-stable.<sup>3</sup> We use the Toomre criterion, and assume that the disc is gravitationally stable when  $Q(R) \equiv c_s \Omega / (\pi G \Sigma) > 1$ . Note that the only effect of radiation pressure is that the sound speed  $c_s$  is computed from the total pressure, not just the gas pressure.

In the radiation pressure-dominated regime of our gray-body disc, the gas volume density *decreases* with increasing surface density, because the disc scale height is a stronger-than-linear function of  $\Sigma$ . This leads to the somewhat counterintuitive behaviour that increasing the surface density in the inner regions of the disc makes it more gravitationally stable. We find that

$$\begin{aligned} R_Q &\equiv R(Q=1) \\ &= 550 \frac{GM}{c^2} \alpha_{0.3}^{34/165} \dot{m}^{62/165} M_9^{-16/55} \theta_{0.2}^{17/55}. \end{aligned} \quad (30)$$

Equation 30 is valid for radiation pressure-dominated regions only; if the surface density is sufficiently low, then gas pressure dominates and decreasing the surface density further increases  $R_Q$ . That is,  $R_Q$  has a minimum value as a function of  $\dot{m} \approx 0.1$  for fiducial disc parameters.

The gas density profile in the outer regions  $R > R_Q$ , where classical thin-disc models predict  $Q < 1$ , is uncertain. One possibility that has been explored by Sirko & Goodman (2003) and others (Thompson, Quataert & Murray 2005; Levin 2007; Lodato et al. 2009) is that feedback mechanisms (such as nuclear fusion from stars that formed in the disc or their supernovae) inject sufficient energy as to maintain marginal gravitational stability with  $Q \approx 1$  in the outer regions. However, the profile of the outer disc is not central to this study, as we are interested in radiation from the central regions of the disc, where the presence of a compact binary is most likely to produce characteristic features that may distinguish them from accretion discs around single SMBHs. To keep our analysis as simple as possible, we simply neglect the thermal radiation of the disc outside  $R_Q$ .

What is the accretion rate in the disc? Uncertainty re-

<sup>3</sup> The gas is susceptible to an additional weak diffusive instability that grows on the Kelvin-Helmholtz timescale,  $t_{\text{KH}} \sim \kappa c_s^2 / (\pi G c)$ . We find that the viscous timescale is shorter than the Kelvin-Helmholtz timescale — i.e., the diffusive instability is irrelevant — in all but the outermost annulus of the radiation-dominated region of our fiducial circumbinary discs (e.g., at  $R = 400 GM/c^2$ ,  $t_{\text{KH}} \sim 2 \times 10^6$  yr and  $t_{\nu} \sim 10^5$  yr). Even in the small region where the disc is formally unstable to the diffusive instability, it is plausible that local turbulence can quench its growth. Hence we assume the diffusive instability is unimportant.



regarding the outer gas distribution notwithstanding, quasars are able to efficiently supply SMBHs of mass  $> 10^8 M_\odot$  with enough fuel to maintain luminosities of  $0.1 - 1 L_{\text{Edd}}$  for periods of  $10^6 - 8$  yr. That most quasars radiate at just under the Eddington limit while few exceed  $L_{\text{Edd}}$  suggests that the accretion rate is limited by radiative feedback, rather than by the availability of fuel. In principle, therefore, the surface density in a circumbinary disc can be significantly greater than in a disc around a solitary SMBH of the same total mass. This is not because of the mass accumulation of gas outside the binary's orbit, but because a circumbinary disc has a much lower luminosity owing to its low-density central cavity. If binary torques inhibit gas from accessing the centre of the potential, then this effectively reduces the radiative efficiency of the system, i.e.  $L_{\text{disc}} \ll \dot{M} c^2$ . We find that even at  $\dot{m} \sim 10$ , the locally viscously dissipated flux in our discs does not provide sufficient radiation pressure to unbind gas from the local gravitational field.<sup>4</sup>

In Figure 3, we plot, for a circumbinary disc around a binary with  $M_0 = 1$ ,  $M_2/M_1 = 1/4$ , several transition radii as a function of the mass accretion parameter  $\dot{m}$ . We show the radii at which the disc transitions from being radiation pressure-dominated to gas pressure-dominated; from where the opacity is dominated by electron scattering to free-free absorption; and from Jeans-stable to unstable. We note that in general, radiation pressure acts to stabilize the disc against Jeans collapse, and that the radius  $R_Q$  closely corresponds to the radius where the disc becomes radiation pressure-dominated. We also plot the size of the cavity  $R_\lambda \sim 2a$  at which the binary's orbital evolution transitions from being gas-driven to GW-driven, and the value of  $R_\lambda$  where  $t_{\text{res}}^{\text{GW}} = t_\nu(R_\lambda)$ . We find that the disc is geometrically thin ( $H/R \ll 1$ ) or marginally thin ( $H/R \lesssim 1$ ) for  $\dot{m} < 10$ .

In conclusion, Figure 3 suggests that a Jeans-stable circumbinary annulus could exist, instantaneously, around an individually resolved PTA source, for any value of the supply rate, extending at least by a factor of two in radius (from the inner radius shown by the [red] dashed line, to the outer radius shown by the [black] dotted curve). However, in order for this annulus to be created through the in-ward migration of the secondary BH from larger radii in a more extended disc, we require that the disc is stable to radii that extend beyond the gas/GW-driven transition. This latter requirement (i.e., the dotted [black] curve must lie above the thick [blue] solid curve) means that in practice, the gaseous annulus exists in PTA sources only if the mass supply rate is  $\dot{m} \gtrsim 1$ . As argued above, while radiative feedback may disallow such high (super-Eddington) rates in thin discs around a single BH, they can naturally be maintained in discs around binaries, owing to their low radiative efficiency.

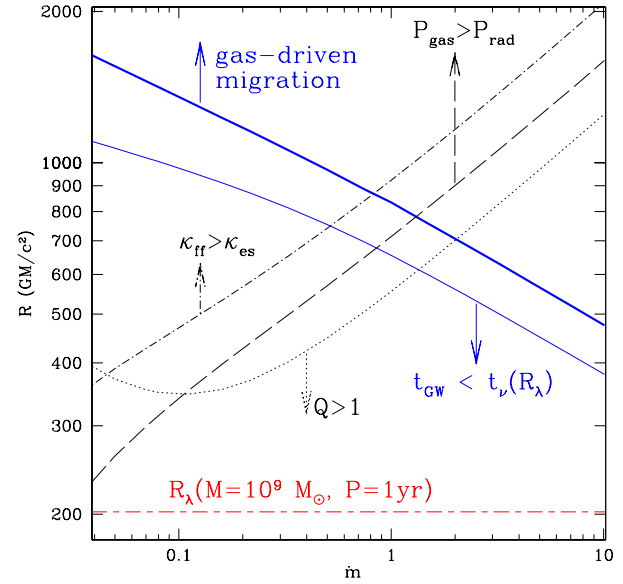


**Figure 3.** In black lines, several transition boundaries within a steady-state, thin accretion disc are plotted as a function of the mass supply rate  $\dot{m} = \dot{M}/(0.1 L_{\text{Edd}}/c^2)$ . Binary parameters are  $M = 10^9 M_\odot$ ,  $M_2/M_1 = 1/4$ ; disc parameters are  $\alpha = 0.3$ ,  $\lambda = 1$ ,  $\theta = 0.2$ . Plotted are the radii in the disc where the disc is marginally stable to gravitational fragmentation ( $R_Q$ ; dotted lines); where the radiation pressure equals the gas pressure (dashed); and where free-free opacity equals electron-scattering opacity (dash-dot). In blue lines, we plot the size of the circumbinary cavity  $R_\lambda = 2a$  where the binary's orbital decay transitions from being gas-driven to GW-driven (thick lines), and when the orbital decay timescale becomes shorter than the viscous timescale at the inner edge of the disc (thin lines). For reference, the radius of the cavity for a  $10^9 M_\odot$  binary with a rest-frame period of 1 yr is plotted as a horizontal red dashed line.

### 3.2 Surface Density Evolution of the Circumbinary Gas

Let us now address the surface density profile of the outer disc at the time when the binary SMBH becomes observable by PTAs.

The tidal torque density  $dT_{\text{tide}}/dR$  is sharply peaked in a narrow region that roughly coincides with the edge of the cavity  $R_\lambda$ , preventing the gas from accreting inward. Everywhere else in the disc, the tidal torques are negligible compared to the viscous torques. The effect of the tidal torques in the region  $R \approx R_\lambda$  can thus be approximated as a boundary condition prohibiting mass flow across  $R_\lambda$  (Pringle 1991; Ivanov, Papaloizou & Polnarev 1999):

$$\dot{M}(R_\lambda, t) = 6\pi\nu\Sigma \left. \frac{\partial \ln(\Sigma R^{1/2})}{\partial \ln R} \right|_{R=R_\lambda} = 0, \quad (31)$$

Note that our disc is not steady-state, and the local mass flow rate  $\dot{M}$  need not be radially constant.

The surface density evolution of the circumbinary disc  $R_\lambda$  is governed by the standard equation for viscous discs (e.g., Pringle 1981; Frank, King & Raine 2002) without including an explicit term for the tidal torques:

$$\frac{\partial}{\partial t} \Sigma(R, t) = \frac{1}{R} \frac{\partial}{\partial R} \left[ R^{1/2} \frac{\partial}{\partial R} (3\nu \Sigma R^{1/2}) \right]. \quad (32)$$

<sup>4</sup> We remind the reader that  $\dot{m}$  is defined with respect to the Eddington limit assuming a radiative efficiency of  $\sim 0.1$ . Strictly speaking, our circumbinary discs are not super-Eddington, even when the parameter  $\dot{m}$  exceeds unity.

A semi-analytic solution for the thin-disc equation 32 with the boundary condition in equation 31 was derived by Tanaka (2011), for a finite boundary  $R_\lambda > 0$  and a special viscosity prescription  $\nu \propto R^n$ . The solution can be written in the form

$$\Sigma(R, t) = \int_{R_\lambda}^{\infty} G(R, R', t; R_\lambda) \Sigma_{\text{init}}(R') dR', \quad (33)$$

where  $G(R, R', t; R_\lambda)$  is the Green's function specific to the boundary condition and the chosen value of the viscosity power-law index  $n$ ; and  $\Sigma_{\text{init}}(R)$  is an arbitrary initial density profile. We find that our discs satisfy  $\nu \propto R^{0.4}$  inside  $R < 10^3 GM/c^2$ , and thus adopt  $n = 0.4$ .

In order to model a thin accretion disc around a GW-driven SMBH binary, we modify the solution of Tanaka (2011) in two ways. First, we derive a more general Green's function to allow for a boundary condition with nonzero mass flux across the inner boundary:

$$\dot{M}(R_\lambda, t) = f_{\text{leak}} \dot{M}_{\text{ss}}(R_\lambda, t). \quad (34)$$

Above,  $\dot{M}_{\text{ss}} = 3\pi\nu\Sigma$  is the standard accretion rate for expected of a steady-state disc, and  $0 \leq f_{\text{leak}} < 1$  is a numerical factor representing the incomplete suppression of gas inflow into the cavity. The case  $f_{\text{leak}} = 0$  corresponds to total suppression of accretion by the binary's tidal torques.

The boundary condition in equation 34 is motivated by results from numerical simulations, which show that in general the binary torques do not completely prevent accretion into the gap, but rather allow some gas to leak into the centre of the disc with a suppressed mass flux  $f_{\text{leak}} \lesssim 0.1$  (e.g., Artymowicz & Lubow 1996; Günther, Schäfer & Kley 2004; Ochi, Sugimoto & Hanawa 2005; MacFadyen & Milosavljević 2008). We choose  $f_{\text{leak}} = 0.1$  as our fiducial value.

The long-term behavior of the gas is to pile up near the cavity and satisfy the power-law  $\nu\Sigma \propto R^{(f_{\text{leak}}-1)/2}$  in the vicinity of the boundary. In comparison, a steady-state around a solitary central mass disc satisfies  $\nu\Sigma = \text{constant}$ , and a boundary condition imposing zero inward mass flux satisfies  $\nu\Sigma \propto R^{-1/2}$  at the boundary. Note, however, that the value of  $f_{\text{leak}}$  does not have a strong effect on the mass profile (and hence the luminosity produced) outside the cavity-opening radius  $R_\lambda$ ; the fractional surface density enhancement due to secondary-dominated migration is typically of order unity.

The gas that enters the cavity does so in nearly radial orbits MacFadyen & Milosavljević (2008), and so is dynamically decoupled from the circumbinary disc. Thus, the surface density and mass flux inside  $R_\lambda$  can consistently be disregarded in the Green's function formalism. The leaked gas can presumably form accretion discs around one or both SMBHs (Hayasaki, Mineshige & Sudou 2007), presumably at the usual AGN radiative efficiency  $\sim 0.1$ . The mass supply rate of such circum-secondary (or -primary) discs will be modulated by  $f_{\text{leak}}\dot{M}_{\text{ss}}$ , which decreases as the binary outruns the circumbinary gas. Because the viscous time at the outer edge of such discs are shorter than at  $R_\lambda$ , they will be nearly steady-state, with the surface density profile at any given time being determined by the instantaneous mass flux into the cavity. Thus, the bolometric luminosities of the discs around each disc may be roughly expressed as  $L < 0.1 f_{\text{leak}}\dot{M}_{\text{ss}}(R_\lambda)c^2$ , and would be Eddington-limited

by the potential of the individual black holes they orbit. This suggests that if the quantity  $f_{\text{leak}}\dot{m}$  exceeds unity, the region inside the cavity would develop radiation-driven outflow winds. Thus, the parameter  $f_{\text{leak}}$  affects the energetic output due to accretion inside the cavity far more than it does that of the circumbinary disc.

The Green's function for the boundary condition in equation 34 is given by

$$\begin{aligned} G(R, R', t; R_\lambda) &= \left(1 - \frac{n}{2}\right) R^{-n-1/4} R'^{5/4} \\ &\times \int_0^\infty \left[ J_\ell(ky) \tilde{Y}_\ell(ky_\lambda) - Y_\ell(ky) \tilde{J}_\ell(ky_\lambda) \right] \\ &\times \left[ J_\ell(ky') \tilde{Y}_\ell(ky_\lambda) - Y_\ell(ky') \tilde{J}_\ell(ky_\lambda) \right] \\ &\times \left[ \tilde{J}_\ell^2(ky_\lambda) + \tilde{Y}_\ell^2(ky_\lambda) \right]^{-1} \\ &\times \exp[-3\Lambda k^2 t] k dk. \end{aligned} \quad (35)$$

Above,  $\ell = 1/(4 - 2n)$  and  $\Lambda = (1 - n/2)^2 \nu R^{-n}$  are constants. We have introduced the variables  $y = R^{1-n/2}$ ,  $y' = R'^{1-n/2}$  and  $y_\lambda = R_\lambda^{1-n/2}$ , as well as the functions

$$\tilde{J}_\ell(x) = x J_{\ell-1}(x) - \frac{f_{\text{leak}}}{2-n} J_\ell(x) \quad \text{and} \quad (36)$$

$$\tilde{Y}_\ell(x) = x Y_{\ell-1}(x) - \frac{f_{\text{leak}}}{2-n} Y_\ell(x). \quad (37)$$

Taking  $f_{\text{leak}} \rightarrow 0$  leads to the solution given in Tanaka (2011; his equation 42) imposing  $\dot{M}(R_\lambda) = 0$ .

The second modification to the Green's function formalism is to allow the inner boundary to move inward as an explicitly known function of time, i.e.,  $R_\lambda(t) = 2\lambda a(t)$ . This is done through a time-weighted superposition of different Green's functions at intermediate values of  $R_\lambda$  (see Appendix).

We take our initial condition as the disc profile when  $t_{\text{res}}^{\text{GW}} = t_\nu(R_\lambda)$ , just as the binary is just beginning to outrun the circumbinary gas. We note that the torques exerted by the disc are not entirely negligible at this stage. For simplicity, we approximate the contribution of the disc torques to the orbital decay rate,  $a/(da/dt)_{\text{disc}} = t_{\text{res}}^{(\text{sec})}$ , as being constant. This is justified as follows. The disc torques are a weak function of  $R_\lambda$ , at least as long as the quantity  $\nu(R_\lambda)\Sigma(R_\lambda)$  is comparable to the steady-state value. Once GW emission dominates the orbital decay, the contribution of disc torques becomes quickly negligible regardless of the value of  $\nu(R_\lambda)\Sigma(R_\lambda)$ .

The orbital decay is then given by

$$\frac{da}{dt} = \left(\frac{da}{dt}\right)_{(\text{GW})} + \left(\frac{da}{dt}\right)_{\text{disc}} = \frac{a}{t_{\text{res}}^{(\text{sec})}} + \frac{64}{5} \frac{c^5}{G^3 M^3} \frac{\eta}{a^3}. \quad (38)$$

With the assumption that  $t_{\text{res}}$  is roughly constant, this has the analytic solution

$$t = \frac{t_{\text{res}}^{(\text{sec})}}{4} \ln \left[ \frac{a_0^4 + 64c^5\eta t_{\text{res}}^{(\text{sec})}/(5G^3 M^3)}{a^4(t) + 64c^5\eta t_{\text{res}}^{(\text{sec})}/(5G^3 M^3)} \right]. \quad (39)$$

In Figure 4, we plot a model surface density profile of the circumbinary disc around a binary with  $M_9 = 1$  and  $M_2/M_1 = 1/4$ . As the initial condition, we take a steady-state surface density profile with  $\dot{m} = 3$ , at the time when  $t_{(\text{GW})} = t_\nu(R_\lambda)$  (solid black curve).<sup>5</sup> Initially, the disc has

<sup>5</sup> Strictly speaking, the surface density profile at this time should

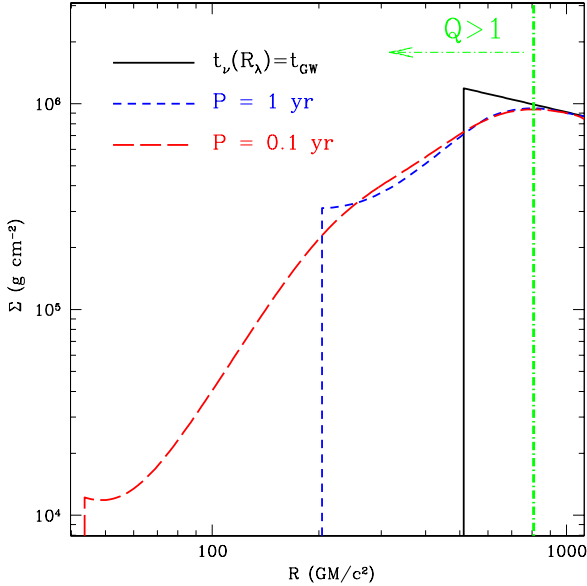


**Figure 4.** The surface density profiles  $\Sigma$  for a circumbinary disc around a PTA source. The binary’s mass is  $10^9 M_\odot$  and its mass ratio is  $M_2/M_1 = 1/4$ . We adopt a moderately high value of the accretion parameter  $\dot{m} = 3$ , and assume that the circumbinary gas can leak into the cavity at the rate given in equation 34, with  $f_{\text{leak}} = 0.1$ . The solid black curve shows the surface density profile when GW emission begins to dominate the binary’s orbital decay ( $t_\nu(R_\lambda) = t_{\text{GW}}$ ,  $R_\lambda = 510 GM/c^2$ ,  $P = 11$  yr). Using the semi-analytic method described in the text, we solve for the surface density profile in the disc at later times, when  $P = 1$  yr (short-dashed blue line) and  $P = 0.1$  yr (long-dashed red line). The dot-dash green line denotes the radius inside which the circumbinary disc is stable against Jeans collapse.

a cavity radius of  $R_\lambda = 510 GM/c^2$  and a rest-frame period of  $P = 11$  yr. We then evolve the profile using our Green’s function to when the orbital period is  $P = 1$  yr (short-dashed blue curve) and  $P = 0.1$  yr (long-dashed red curve). We denote with a green dot-dashed line the radius where  $Q = 1$ , beyond which the disc is expected to be susceptible to the Jeans instability. All the disc profiles are truncated at twice the binary’s semi-major axis, and lose mass across this radius through the boundary condition in equation 34, with  $f_{\text{leak}} = 0.1$ . Note that the boundary radius  $R_\lambda$  moves inward faster than the gas can pile up. We see that a small amount of gas is able to follow the binary’s orbital decay, even though the bulk of the circumbinary disc is getting left behind by the inspiraling binary.

deviate somewhat from the steady-state one. During secondary-dominated migration, the circumbinary surface density profile  $\Sigma(R \gtrsim R_\lambda)$  can become greater than the steady-state profile by at most a factor of  $\sim 1.4$  (equation 28; note that the pileup must be smaller if one accounts for the fact that  $f_{\text{leak}} > 0$ ). Prior to our initial condition, GW emission accelerates the binary’s orbital evolution, and the circumbinary pileup spreads out; however, the surface density does not decrease below the steady-state profile, since  $t_{\text{res}} > t_\nu(R_\lambda)$ . A difference in  $\Sigma$  of less than 40% is insignificant compared to the other theoretical uncertainties, and we employ the steady-state profile for simplicity.

### 3.3 Thermal Emission of Accreting PTA Sources

Since the innermost gas is missing from the accretion discs around PTA binaries, it is probable that their accretion flows will emit less UV and thermal X-rays compared to ordinary AGN powered by solitary BHs. The question then is how UV- and X-ray-deficient these objects are; the answer depends on how much gas is able to follow the binary’s decaying orbit, and how much of this gas is further able to leak into the cavity and accrete onto individual SMBHs. This is a complex problem characterized by dynamical richness in 3D, and considerable theoretical uncertainty of the underlying fluid physics. With the above caveat in mind, we will use as a first approximation the toy surface density evolution model introduced in §3.2 to estimate the thermal emission from an accreting PTA source.

In Figure 5, we show the thermal spectrum for a  $M_9 = 1$ ,  $M_2/M_1 = 1/4$  PTA source, calculated from the circumbinary gas surface density profiles in Figure 4. We have plotted (i) the circumbinary disc with  $\dot{m} = 3$  inside the radius where  $Q = 1$  (dotted, left hump); (ii) an accretion disc around the secondary SMBH (dotted, right hump) fueled by leakage into the cavity and truncated at the Hill radius, for which we use  $R_H \sim 0.5\eta^{1/3}a$ ; and (iii) the combined emission of the two discs (solid thick line). For comparison, we also show the spectrum for an Eddington-limited thin disc (dashed lines) around a solitary SMBH with the same mass as the binary. For simplicity, we have assumed that all of the gas leaked into the cavity fuels a circum-secondary disc. We have plotted spectra when the source has a binary orbital period of  $P = 1$  yr and when  $P = 0.1$  yr.

The result is what would be expected intuitively. The infrared and optical flux, which is produced almost exclusively in the circumbinary disc, does not vary greatly from what is expected from a standard thin disc. However, the flux drops precipitously below wavelengths of  $\lambda \lesssim 3000 \text{ \AA}$  ( $\nu > 10^{15}$  Hz in the figure). This is in stark contrast to most unobscured quasars thought to be powered by  $\sim 10^{8-9} M_\odot$  SMBHs, which have their *brightest* emission in the rest-frame near-UV near their Lyman- $\alpha$  line. The bolometric luminosity of the accreting PTA source is roughly  $\sim 0.03 L_{\text{Edd}}$  for  $P = 1$  yr, and  $\sim 10^{-3} L_{\text{Edd}}$  for  $P = 0.1$  yr. The optical and infrared emission is dominated by the circumbinary disc, whereas the UV and X-rays are produced by circum-secondary accretion fueled by leakage of circumbinary gas into the cavity. As the binary evolves toward shorter periods, the circum-secondary disc is depleted — the viscous time at the Hill radius is typically a few hundred years, shorter than the time to binary merger — and as a result, less gas is able to leak into the cavity, decreasing the UV and X-ray emission. The degree to which the UV and X-ray emission is suppressed depends on the model parameters (in particular  $f_{\text{leak}}$ ) and on the binary period.

We also note that the downturn in the near-UV flux at  $\lambda \lesssim 300 \text{ nm}$  could help distinguish PTA sources from single-SMBH AGN. This feature will be observable in the optical if the source redshift is high; e.g., at  $z = 1$  it will be in the V band. Hence, even in the optical, this source will have an unusual color: it will appear fainter in the U and B bands than a typical AGN. The downturn could be distinguished from reddening due to dust obscuration through the deviation from the power-law spectral shape of dust reddening.

We propose that once an individually resolved PTA source is detected and its error box determined, searching for AGN with weak UV emission lines (e.g., Ly  $\alpha$ ) and/or weak soft X-ray emission is a promising method to narrow the field of interlopers. AGN whose soft X-ray fluxes are weaker by more than a factor of 10 compared to the average have indeed been detected, and are estimated to constitute at most  $\sim 1\%$  of the general AGN population (e.g., Brandt, Laor & Wills 2000; Leighly et al. 2007; Gibson, Brandt & Schneider 2008; Wu et al. 2011, and refs. therein). There have also been observations of quasars with exceptionally weak lines (Diamond-Stanic et al. 2009); these objects have infrared and optical emission consistent with those of typical luminous AGN, and also tend to be X-ray weak (Shemmer et al. 2009). That X-ray weak AGN are so rare suggests that it will be possible to narrow the number of interlopers in a typical PTA error box by a factor of  $\approx 100$ , i.e. either to a handful of objects, or yielding a unique EM counterpart candidate. It is possible, furthermore, that some of these rare X-ray weak AGN are in fact the SMBH binaries PTAs will be detecting.

Our results also strongly suggest that AGN counterparts to PTA sources should draw from optically selected surveys, as their nature makes them likely to be missed by X-ray searches (see, however, Sesana et al. 2011, who investigate the possible X-ray searches of PTA source binaries that have not yet decoupled). The *Large Synoptic Survey Telescope*<sup>6</sup> should be able to detect all of the optically luminous AGN in the PTA error box within  $z \sim 1$ . It may be possible to follow up candidates individually, but comparing the optical data with that of wide-field X-ray surveys such as *MAXI*<sup>7</sup>, *eROSITA*<sup>8</sup> or *Wide Field X-ray Telescope*<sup>9</sup> would greatly facilitate the multi-wavelength search for counterpart candidates inside the error box.

Additional follow-up studies of candidates may further corroborate the identification of a counterpart. For example, the gas that leaks radially into the cavity can shock-heat the outer edge of the circum-secondary (or circum-primary) disc and produce hot spots. The viscously dissipated luminosity of a circum-secondary disc is roughly  $L_{\text{disc}2} \lesssim (1/2)GM_2\dot{M}_2/R_{\text{ISCO},2}$ , where  $M_2 \leq f_{\text{leak}}\dot{M}(R_\lambda)$  is the mass supply rate of the circum-secondary disc and  $R_{\text{ISCO},2}$  is the radius of innermost stable circular orbit around the secondary. The time-averaged power per unit mass of the hot spots is limited by the amount of kinetic energy the flow can deposit at the outer edge of the circum-secondary disc, i.e.  $L_{\text{hot}} \lesssim GM_2\dot{M}_2/R_H$ . It follows directly that the time-averaged ratio between between the hot-spots and the intrinsic luminosity of the circum-secondary disc is

$$\frac{L_{\text{hot}}}{L_{\text{disc}2}} \lesssim \frac{R_{\text{ISCO},2}}{R_H} \sim \eta^{-1/3} \frac{R_{\text{ISCO},2}}{a} \gtrsim \left( \frac{a}{GM/c^2} \right)^{-1}. \quad (40)$$

In other words, the time-averaged power of a hot spot is of order  $\gtrsim 1 - 10\%$  of the circum-secondary disc luminosity for resolved PTA sources. In principle, the luminosity of any single flare could be much greater. Because streaming into the cavity is expected to be modulated quasi-periodically by the

binary's orbital period (e.g., Hayasaki, Mineshige & Sudou 2007; MacFadyen & Milosavljević 2008), EM counterparts of resolved PTA sources may be characterized by periodic UV flares.

In the same vein, if the orbital plane lies close to the line of sight, the UV lines would display strong periodic Doppler shifting with respect to the optical emission, modulated at the binary's orbital period (e.g., Halpern & Filippenko 1988). Thus, monitoring candidate counterparts for periodic or quasi-periodic variability on orbital timescales may prove a fruitful route for identification Haiman, Kocsis & Menou (2009). As a proof of this concept, we note that Boroson & Lauer (2009) recently reported a candidate SMBH binary, with two sets of broad emission lines separated by  $3,500 \text{ km s}^{-1}$ , with inferred component masses of  $M_1 = 10^{8.9} M_\odot$  and  $M_2 = 10^{7.3} M_\odot$ . The binary interpretation, however, could be ruled out by the lack of any change in the velocity offset between two spectra taken  $\approx 1$  year apart (Chornock et al. 2009).

Lastly, we consider the scenario of Chang et al. (2010), in which the circum-primary disc brightens prior to merger due to tidal excitation by the shrinking binary. The power generated by this process can be approximated as (see their equation 15)

$$\begin{aligned} L_{\text{tide}} &\sim \frac{GMM_{\text{in}}}{2at_{\text{merge}}} \\ &\sim 1.4 \times 10^{43} M_9^{7/3} \eta_{1:4} P_1^{-10/3} \frac{M_{\text{in}}}{100 M_\odot} \text{erg s}^{-1}, \quad (41) \end{aligned}$$

where  $M_{\text{in}}$  is the mass of the circum-primary disc. Extrapolation of the Chang et al. (2010) results to binaries with mass  $M \sim 10^9 M_\odot$  (their calculations only considered binaries up to  $M = 10^8 M_\odot$ ) suggests a value of  $M_{\text{in}} \sim 100 M_\odot$ . Similar values are obtained by estimating the disc mass that can be fueled by gas leaking into the cavity with  $f_{\text{leak}} \sim 0.1$ , when the time to merger is comparable to the viscous timescale at the outer edge of the circum-primary disc.

Equation 41 suggests that the power produced by tidal excitation of the circum-primary disc is negligible compared to the thermal disc emission if the binary period is  $P \sim 1$  yr. However, for sources with  $P \sim 0.1$  yr, the tidally excited emission would rival the bolometric output of the thermal emission. The tidal component, which would have a peak frequency in the UV and soft X-rays, will brighten dramatically prior to merger on timescales of several years to decades. Even though  $P \sim 0.1$  yr sources are predicted to be much rarer and also much more difficult to resolve individually with PTAs, they present tantalizing possibilities for observing EM signatures that are directly related to binary coalescence.

## 4 CONCLUSIONS

In this paper we considered the possibility that individually resolved PTA sources — SMBH binaries with  $M \sim 10^9 M_\odot$ ,  $M_2/M_1 \sim 1/4$ ,  $P \sim 0.1 - 1$  yr and  $z \lesssim 1.5$  — may be identified with EM observations if they reside in gas-rich environments. Multi-wavelength observations of such systems would allow for studies of an AGN in a system that is known to harbour a compact SMBH binary, thus pro-

<sup>6</sup> <http://www.lsst.org/lsst>

<sup>7</sup> <http://maxi.riken.jp/top/>

<sup>8</sup> <http://www.mpe.mpg.de/erosita/>

<sup>9</sup> <http://www.wfxt.eu/home/Overview.html>

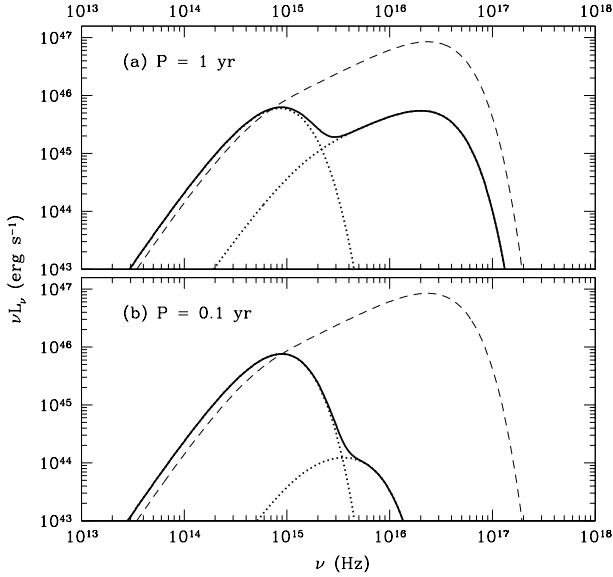


**Figure 5.** We plot the spectral energy distribution from the thin, viscous circumbinary accretion disc from Figure 4 (red curve;  $M = 10^9 M_\odot$ ,  $P = 1$  yr), when the source has a period (a)  $P = 1$  yr and (b)  $P = 0.1$  yr. We assume that some of the gas at the cavity/disc boundary is able to accrete into the cavity at a suppressed rate and fuel a small accretion disc around the secondary SMBH (see text for details). The spectra from individual discs are shown in dotted lines, with the circumbinary cavity emitting at lower frequencies. The combined spectrum from the circumbinary and circum-secondary accretion discs is shown in solid thick lines. We plot for reference the model AGN spectrum (thin dashed) for an Eddington-limited thin disc around a single SMBH with the same mass as the binary. The spectra for the PTA source are UV and X-ray weak compared to a standard thin disc model around a single SMBH. However, the infrared and optical emission, mostly produced in the circumbinary disc, is similar to what would be expected for a single-SMBH disc.

viding a unique window into gas accretion in a rapidly time-varying gravitational potential. If, as suggested by Corbin & Cornish (2010), PTAs can constrain the luminosity distance to individually resolved sources, these SMBHs can be used as “standard sirens” to measure the cosmic expansion history. Interestingly, the predicted redshift distribution of these sources lies between  $0.1 \lesssim z \lesssim 1.5$ , comparable to that of the deepest Type-Ia supernovae surveys, and a range where *LISA* detection rates are expected to be low (Sesana, Volonteri & Haardt 2007).

Our findings can be summarized as follows:

- The number of interloping massive halos and AGN that may be confused with the PTA source is typically  $N_g \sim 10^4$  for a  $10^9 M_\odot$  binary if the contributions to the signal from individual pulsars are not identifiable in the PTA data.
- In the more optimistic case, the pulsar term can be constrained and utilized to better determine the sky location of the source as well as constrain its redshift and mass. The number of interlopers can then drop to  $N_g \sim 10 - 100$  at  $z \sim 0.5$ , and perhaps to  $N < 1$  for close sources at redshifts as close as  $z \lesssim 0.2$ .
- By considering the orbital evolution history of an

accreting PTA source, first by tidal interactions with the circumbinary gas and then by GW emission, we showed that a gaseous accretion disc around the source can be expected to be gas-poor both inside and immediately outside its orbit. They would thus have optical and infrared luminosities comparable with typical quasars, while exhibiting low soft X-ray luminosities and weak UV emission lines. The downturn in flux below 300 nm could be discerned by optical observations if the source redshift is  $z \gtrsim 1$ . Searching for AGN in the PTA error box with one or more of these atypical characteristics could lead to the identification of a single EM counterpart. Further monitoring candidate counterparts for periodicity and other theoretically predicted pre-coalescence signatures may also aid identification.

## ACKNOWLEDGMENTS

As we were completing this work, we became aware of a concurrent independent study by Sesana et al. (2011), addressing similar questions. TT acknowledges fruitful discussions with Alberto Sesana, Massimo Dotti, and Constanze Rödig. The authors also thank Jules Halpern and Jeremy Goodman for insightful conversations. This work was supported by NASA ATFP grants NNX08AH35G (to KM) and NNX10ZDA001N (to ZH) and by the Polányi Program of the Hungarian National Office for Research and Technology (NKTH; to ZH). This research was supported in part by the Perimeter Institute for Theoretical Physics.

# APPENDIX: GREEN'S-FUNCTION SOLUTION FOR THE THIN-DISC EQUATION WITH MOVING INNER BOUNDARIES

Consider a disc at time  $t$  which has surface density profile  $\Sigma(R, t)$  and moving inner boundary  $R_\lambda(t)$ . During an infinitesimal time-step  $\Delta t$ , the boundary moves to  $R_\lambda + \Delta R_\lambda = R_\lambda(t + \Delta t) < R_\lambda$ , and the surface density evolves to

$$\Sigma(R, t + \Delta t) = \int_{R_\lambda + \Delta R_\lambda}^{\infty} G(R, R', t + \Delta t; R_\lambda + \Delta R_\lambda) \Sigma_{\text{init}}(R') dR'. \quad (42)$$

From equations 33 and 42, we may write the derivative  $d\Sigma/dt$  through its definition.

$$\begin{aligned} \frac{d}{dt} \Sigma(R, t) &\equiv \lim_{\Delta t \rightarrow 0} \frac{\Sigma(R, t + \Delta t) - \Sigma(R, t)}{\Delta t} \\ &= \lim_{\Delta t \rightarrow 0} \left[ \int_{R_\lambda + \Delta R_\lambda}^{\infty} \frac{G(R, R', t + \Delta t; R_\lambda + \Delta R_\lambda)}{\Delta t} \Sigma_{\text{init}}(R') dR' - \int_{R_\lambda}^{\infty} \frac{G(R, R', t; R_\lambda)}{\Delta t} \Sigma_{\text{init}}(R') dR' \right] \\ &= \lim_{\Delta t \rightarrow 0} \int_{R_\lambda}^{\infty} \left[ \frac{G(R, R', t + \Delta t; R_\lambda + \Delta R_\lambda)}{\Delta t} - \frac{G(R, R', t; R_\lambda)}{\Delta t} \right] \Sigma_{\text{init}}(R') dR' \\ &\quad + \lim_{\Delta t \rightarrow 0} \int_{R_\lambda + \Delta R_\lambda}^{R_\lambda} \frac{G(t + \Delta t; R_\lambda + \Delta R_\lambda)}{\Delta t} \Sigma_{\text{init}}(R') dR'.. \end{aligned} \quad (43)$$

The last term evaluates to

$$\lim_{\Delta t \rightarrow 0} \frac{R_\lambda(t) - R_\lambda(t + \Delta t)}{\Delta t} G(R, R_\lambda, t; R_\lambda) \Sigma_{\text{init}}(R_\lambda) = -\frac{dR_\lambda}{dt} G(R, R_\lambda, t; R_\lambda) \Sigma_{\text{init}}(R_\lambda), \quad (44)$$

which must be zero for all  $t > 0$  since the initial surface density profile is zero inside  $R_\lambda(t = 0)$ . We are left with

$$\begin{aligned} \frac{d}{dt} \Sigma(R, t) &= \lim_{\Delta t \rightarrow 0} \int_{R_\lambda}^{\infty} \left[ \frac{G(R, R', t + \Delta t; R_\lambda(t + \Delta t))}{\Delta t} - \frac{G(R, R', t; R_\lambda)}{\Delta t} \right] \Sigma_{\text{init}}(R') dR' \\ &= \int_{R_\lambda(t)}^{\infty} \left[ \frac{\partial G(R, R', t; R_\lambda)}{\partial t} + \frac{\partial G(R, R', t; R_\lambda)}{\partial R_\lambda} \frac{dR_\lambda}{dt} \right] \Sigma_{\text{init}}(R') dR'. \end{aligned} \quad (45)$$

Equation 45 is an ordinary differential equation with respect to the variable  $t$ . We wish to begin with an initial condition  $\Sigma_{\text{init}}(R)$  and integrate to a subsequent time  $t^*$ , with  $R_\lambda^* = R_\lambda(t^*)$ . In the context of this paper, the initial condition is the point when the binary's orbital decay becomes GW-driven, and  $t^*$  is the time when the system is observed as an individually resolved PTA source and  $R_\lambda(t) \geq R_\lambda^*$  describes the (GW-driven) evolutionary history of the gap-opening radius prior to  $t^*$ .

Direct integration gives the expression

$$\Sigma(R, t^*) = \Sigma_{\text{init}}(R') + \int_0^{t^*} \int_{R_\lambda(t)}^{\infty} \left[ \frac{\partial G(R, R', t; R_\lambda)}{\partial t} + \frac{\partial G(R, R', t; R_\lambda)}{\partial R_\lambda} \frac{dR_\lambda}{dt} \right] \Sigma_{\text{init}}(R') dR' dt. \quad (46)$$

We may write this in the form of a Green's function,

$$\Sigma(R, t) = \int_0^{\infty} \mathcal{G}(R, R', t^*) \Sigma_{\text{init}}(R') dR', \quad (47)$$

where

$$\mathcal{G}(R, R', t^*) = \delta(R - R') + \int_0^{t^*} \left[ \frac{\partial G(R, R', t; R_\lambda)}{\partial t} + \frac{\partial G(R, R', t; R_\lambda)}{\partial R_\lambda} \frac{dR_\lambda}{dt} \right] dt. \quad (48)$$

Note that  $G = 0$  for all  $R < R_\lambda$  and  $R' < R_\lambda$ . The Dirac  $\delta$ -function can be awkward to implement in a numerical integration scheme. We rewrite it in terms of the known Green's function with a fixed boundary by using the fact that any Green's function evaluated at  $t = 0$  is the  $\delta$ -function, i.e.,

$$G(R, R', t^*; R_\lambda^*) = \delta(R - R') + \int_0^{t^*} \frac{\partial G(R, R', t; R_\lambda^*)}{\partial t} dt. \quad (49)$$

We thus obtain for our “master” Green's function:

$$\mathcal{G}(R, R', t^*) = G(R, R', t^*; R_\lambda^*) + \int_0^{t^*} \left[ \frac{\partial G(R, R', t; R_\lambda)}{\partial t} - \frac{\partial G(R, R', t; R_\lambda^*)}{\partial t} + \frac{\partial G(R, R', t; R_\lambda)}{\partial R_\lambda} \frac{dR_\lambda}{dt} \right] dt. \quad (50)$$

We see that if the boundary is stationary, the second term above vanishes and  $\mathcal{G} = G$ . Note the similarity of the mathematical form of our solution to DuHamel's theorem (e.g., Carslaw & Jaeger 1959) for time-dependent boundary conditions. This is not surprising, given that both are based on the superposition principle. For our thin accretion disc problem, the function  $\mathcal{G}(R, R', t)$  is explicitly known and easily tabulated, given a specific combination of: (i) the parameter  $f_{\text{leak}}$ ; (ii) boundary evolution  $R_\lambda(t)$ ; and (iii) viscous power-law index  $\nu(R) \propto R^n$ , with  $n < 2$ .

## REFERENCES

- Armitage P. J., Natarajan P., 2002, *ApJ*, 567, L9  
—, 2005, *ApJ*, 634, 921  
Artymowicz P., Clarke C. J., Lubow S. H., Pringle J. E., 1991, *ApJ*, 370, L35  
Artymowicz P., Lubow S. H., 1994, *ApJ*, 421, 651  
—, 1996, *ApJ*, 467, L77+  
Baker J. G., Centrella J., Choi D., Koppitz M., van Meter J., 2006, *Phys. Rev. Lett.*, 96, 111102  
Barnes J. E., Hernquist L. E., 1991, *ApJ*, 370, L65  
Bate M. R., Lubow S. H., Ogilvie G. I., Miller K. A., 2003, *MNRAS*, 341, 213  
Blaes O. M., 2004, in *Accretion Discs, Jets and High Energy Phenomena in Astrophysics*, V. Beskin, G. Henri, F. Menard, & et al., ed., pp. 137–185  
Blecha L., Loeb A., 2008, *MNRAS*, 390, 1311  
Bogdanović T., Eracleous M., Sigurdsson S., 2009, *ApJ*, 697, 288  
Bogdanović T., Smith B. D., Sigurdsson S., Eracleous M., 2008, *ApJS*, 174, 455  
Bonoli S., Shankar F., White S. D. M., Springel V., Wyithe J. S. B., 2010, *MNRAS*, 404, 399  
Borson T. A., Lauer T. R., 2009, *Nature*, 458, 53  
Brandt W. N., Laor A., Wills B. J., 2000, *ApJ*, 528, 637  
Callegari S., Mayer L., Kazantzidis S., Colpi M., Governato F., Quinn T., Wadsley J., 2009, *ApJ*, 696, L89  
Campanelli M., Lousto C. O., Marronetti P., Zlochower Y., 2006, *Phys. Rev. Lett.*, 96, 111101  
Carlberg R. G., 1990, *ApJ*, 350, 505  
Carslaw H. S., Jaeger J. C., 1959, *Conduction of heat in solids*  
Chang P., Strubbe L. E., Menou K., Quataert E., 2010, *MNRAS*, 1003  
Chornock R. et al., 2009, *The Astronomer’s Telegram*, 1955, 1  
Colpi M., Callegari S., Dotti M., Mayer L., 2009, *Class. Quantum Grav.*, 26, 094029  
Corbin V., Cornish N. J., 2010, *arXiv e-prints*, 1008.1782 (CC10)  
Cuadra J., Armitage P. J., Alexander R. D., Begelman M. C., 2009, *MNRAS*, 393, 1423  
Diamond-Stanic A. M. et al., 2009, *ApJ*, 699, 782  
Donovan J. L., Hibbard J. E., van Gorkom J. H., 2007, *AJ*, 134, 1118  
Dotti M., Montuori C., Decarli R., Volonteri M., Colpi M., Haardt F., 2009, *MNRAS*, 398, L73  
Dotti M., Salvaterra R., Sesana A., Colpi M., Haardt F., 2006, *MNRAS*, 372, 869  
Dutton A. A., Conroy C., van den Bosch F. C., Prada F., More S., 2010, *MNRAS*, 407, 2  
Escala A., Larson R. B., Coppi P. S., Mardones D., 2005, *ApJ*, 630, 152  
Fakhouri O., Ma C., 2009, *MNRAS*, 394, 1825  
Ferrarese L., Merritt D., 2000, *ApJ*, 539, L9  
Floyd D. J. E., Kukulka M. J., Dunlop J. S., McLure R. J., Miller L., Percival W. J., Baum S. A., O’Dea C. P., 2004, *MNRAS*, 355, 196  
Frank J., King A., Raine D. J., 2002, *Accretion Power in Astrophysics: Third Edition*. Cambridge University Press  
Gabasch A. et al., 2004, *A&A*, 421, 41  
—, 2006, *A&A*, 448, 101  
Gaskell C. M., 1996, *ApJ*, 464, L107+  
Gebhardt K. et al., 2000, *ApJ*, 539, L13  
Gibson R. R., Brandt W. N., Schneider D. P., 2008, *ApJ*, 685, 773  
Giocoli C., Tormen G., Sheth R. K., van den Bosch F. C., 2010, *MNRAS*, 404, 502  
Goldreich P., Tremaine S., 1980, *ApJ*, 241, 425  
Governato F. et al., 2009, *MNRAS*, 398, 312  
Gültekin K. et al., 2009, *ApJ*, 698, 198  
Günther R., Schäfer C., Kley W., 2004, *A&A*, 423, 559  
Haiman Z., Kocsis B., Menou K., 2009, *ApJ*, 700, 1952  
Haiman Z., Kocsis B., Menou K., Lippai Z., Frei Z., 2009, *Classical and Quantum Gravity*, 26, 094032  
Halpern J. P., Filippenko A. V., 1988, *Nature*, 331, 46  
Häring N., Rix H.-W., 2004, *ApJ*, 604, L89  
Hayasaki K., 2009, *PASJ*, 61, 65  
Hayasaki K., Mineshige S., Sudou H., 2007, *PASJ*, 59, 427  
Hernquist L., 1989, *Nature*, 340, 687  
Hernquist L., Mihos J. C., 1995, *ApJ*, 448, 41  
Hirata C. M., Holz D. E., Cutler C., 2010, *PRD*, 81, 124046  
Hirose S., Blaes O., Krolik J. H., 2009, *ApJ*, 704, 781  
Hirose S., Krolik J. H., Blaes O., 2009, *ApJ*, 691, 16  
Holz D. E., Hughes S. A., 2005, *ApJ*, 629, 15  
Hopkins P. F., Bundy K., Hernquist L., Ellis R. S., 2007, *ApJ*, 659, 976  
Hopkins P. F., Hernquist L., Cox T. J., Kereš D., 2008, *ApJS*, 175, 356  
Hopkins P. F., Richards G. T., Hernquist L., 2007, *ApJ*, 654, 731  
Ivanov P. B., Papaloizou J. C. B., Polnarev A. G., 1999, *MNRAS*, 307, 79  
Jarosik N. et al., 2011, *ApJS*, 192, 14  
Jenkins A., Frenk C. S., White S. D. M., Colberg J. M., Cole S., Evrard A. E., Couchman H. M. P., Yoshida N., 2001, *MNRAS*, 321, 372  
Kauffmann G., Haehnelt M., 2000, *MNRAS*, 311, 576  
Kocsis B., Frei Z., Haiman Z., Menou K., 2006, *ApJ*, 637, 27  
Kocsis B., Haiman Z., Menou K., 2008, *ApJ*, 684, 870  
Kocsis B., Haiman Z., Menou K., Frei Z., 2007, *PRD*, 76, 022003  
Kocsis B., Sesana A., 2011, *MNRAS*, 411, 1467  
Kollmeier J. A. et al., 2006, *ApJ*, 648, 128  
Kormendy J., Richstone D., 1995, *ARAA*, 33, 581  
Lang R. N., Hughes S. A., 2006, *PRD*, 74, 122001  
—, 2008, *ApJ*, 677, 1184  
Lauer T. R. et al., 2007, *ApJ*, 662, 808  
Leighly K. M., Halpern J. P., Jenkins E. B., Grupe D., Choi J., Prescott K. B., 2007, *ApJ*, 663, 103  
Levin Y., 2007, *MNRAS*, 374, 515  
Lightman A. P., Eardley D. M., 1974, *ApJ*, 187, L1+  
Lin L. et al., 2010, *ApJ*, 718, 1158  
—, 2008, *ApJ*, 681, 232  
Lodato G., Nayakshin S., King A. R., Pringle J. E., 2009, *MNRAS*, 398, 1392  
MacFadyen A. I., Milosavljević M., 2008, *ApJ*, 672, 83  
Magorrian J. et al., 1998, *AJ*, 115, 2285  
Makino J., 1997, *ApJ*, 478, 58  
Mayer L., Kazantzidis S., Madau P., Colpi M., Quinn T., Wadsley J., 2007, *Science*, 316, 1874  
McWilliams S. T., Thorpe J. I., Baker J. G., Kelly B. J., 2010, *PRD*, 81, 064014



- Mihos J. C., Hernquist L., 1996, *ApJ*, 464, 641
- Milosavljević M., Merritt D., Rest A., van den Bosch F. C., 2002, *MNRAS*, 331, L51
- Milosavljević M., Phinney E. S., 2005, *ApJ*, 622, L93
- Ochi Y., Sugimoto K., Hanawa T., 2005, *ApJ*, 623, 922
- Paczynski B., 1978, *ACTAA*, 28, 91
- Percival W. J., Miller L., McLure R. J., Dunlop J. S., 2001, *MNRAS*, 322, 843
- Peters P. C., 1964, *Physical Review*, 136, 1224
- Piran T., 1978, *ApJ*, 221, 652
- Pretorius F., 2005, *Phys. Rev. Lett.*, 95, 121101
- Pringle J. E., 1976, *MNRAS*, 177, 65
- , 1981, *ARAA*, 19, 137
- , 1991, *MNRAS*, 248, 754
- Ravindranath S., Ho L. C., Filippenko A. V., 2002, *ApJ*, 566, 801
- Roedig C., Dotti M., Sesana A., Cuadra J., Colpi M., 2011, *MNRAS*, 979
- Sánchez-Blázquez P., Gibson B. K., Kawata D., Cardiel N., Balcells M., 2009, *MNRAS*, 400, 1264
- Sanders D. B., Soifer B. T., Elias J. H., Madore B. F., Matthews K., Neugebauer G., Scoville N. Z., 1988, *ApJ*, 325, 74
- Schawinski K., Treister E., Urry C. M., Cardamone C. N., Simmons B., Yi S. K., 2011, *ApJ*, 727, L31+
- Schechter P., 1976, *ApJ*, 203, 297
- Schnittman J. D., 2011, *Classical and Quantum Gravity*, 28, 094021
- Schutz B. F., 1986, *Nature*, 323, 310
- Sesana A., Roedig C., Reynolds M. T., Dotti M., 2011, *arXiv e-prints*, 1107.2927
- Sesana A., Vecchio A., 2010, *PRD*, 81, 104008 (SV10)
- Sesana A., Vecchio A., Volonteri M., 2009, *MNRAS*, 394, 2255
- Sesana A., Volonteri M., Haardt F., 2007, *MNRAS*, 377, 1711
- Shakura N. I., Sunyaev R. A., 1976, *MNRAS*, 175, 613
- Shang C., Haiman Z., 2011, *MNRAS*, 411, 9
- Shemmer O., Brandt W. N., Anderson S. F., Diamond-Stanic A. M., Fan X., Richards G. T., Schneider D. P., Strauss M. A., 2009, *ApJ*, 696, 580
- Shen Y., Loeb A., 2010, *ApJ*, 725, 249
- Sirko E., Goodman J., 2003, *MNRAS*, 341, 501
- Springel V. et al., 2005, *Nature*, 435, 629
- Tanaka T., 2011, *MNRAS*, 410, 1007
- Tanaka T., Haiman Z., Menou K., 2010, *AJ*, 140, 642
- Tanaka T., Menou K., 2010, *ApJ*, 714, 404
- Tang S., Grindlay J., 2009, *ApJ*, 704, 1189
- Thompson T. A., 2008, *ApJ*, 684, 212
- Thompson T. A., Quataert E., Murray N., 2005, *ApJ*, 630, 167
- Tremaine S. et al., 2002, *ApJ*, 574, 740
- Tundo E., Bernardi M., Hyde J. B., Sheth R. K., Pizzella A., 2007, *ApJ*, 663, 53
- Turner N. J., 2004, *ApJ*, 605, L45
- van Dokkum P. G., 2005, *AJ*, 130, 2647
- Vecchio A., 2004, *PRD*, 70, 042001
- Volonteri M., Madau P., Haardt F., 2003, *ApJ*, 593, 661
- Wu J. et al., 2011, *arXiv e-prints*, 1104.3861
- Wyithe J. S. B., Loeb A., 2003, *ApJ*, 590, 691
- Zakamska N. L. et al., 2006, *AJ*, 132, 1496
- Zhou H., Wang T., Zhang X., Dong X., Li C., 2004, *ApJ*, 604, L33